INSTITUTE OF PHYSICS PUBLISHING JOURNAL OF PHYSICS: CONDENSED MATTER

J. Phys.: Condens. Matter **15** (2003) 7953–7979 PII: S0953-8984(03)69077-6

Frank–Kasper polyhedra, disclination nets and basic magnetism in $Nd_3(Fe, Ti)_{29}$ and $Nd_3(Fe, Ti)_{29}N_x$ intermetallics

V Psycharis[1] **and C Christides**[2,3]

[1] Institute of Materials Science, National Centre for Scientific Research 'Demokritos', 153 10 Athens, Greece
[2] Department of Engineering Sciences, School of Engineering, University of Patras, 26 500 Patras, Greece

E-mail: christides@ims.demokritos.gr

Received 16 September 2003
Published 7 November 2003
Online at stacks.iop.org/JPhysCM/15/7953

Abstract

High-precision crystal structure parameters have been determined from Rietveld refinement of high-resolution neutron powder diffraction data in $Nd_3(Fe, Ti)_{29}$ and $Nd_3(Fe, Ti)_{29}N_x$ intermetallics. The construction of the corresponding Wigner–Seitz (WS) polyhedra has revealed that some 12-fold (group-A) environments and the 14-fold (group-D, dumbbell) environments remain intact upon nitrogen uptake whereas some other 12-fold (group-B, C) environments transform according to the Frank–Kasper sequence $[0, 0, 12, 0] \rightarrow [0, 1, 10, 2]$. For comparison, WS cells were calculated for the 12-, 13-and 14-fold Frank–Kasper-like polyhedra of 1:12 and 2:17 types of structure. A global character of WS volume (WSV) relations has been revealed, where the corresponding WSVs follow the same trend for the three types of structure. Disclination nets have been constructed for the three types of structure, revealing that the easy-magnetization direction (EMD) of the iron sublattice is always along the [–Nd–Fe–] type of disclination line. A comparative analysis of the site hyperfine fields B^i_{hf} in the three kinds of compound led to successful estimations of saturation magnetization (M_s(Fe) = 42.6 μ_B/fu) from Fe-site magnetic moments for $Nd_3Fe_{27.3}Ti_{1.7}$($\equiv Nd_2Fe_{16.3}Ti_{0.7} + NdFe_{11}Ti$) and its nitride ($M_s$(Fe) = 52.8 μ_B/fu) at room temperature. The successful prediction of Fe-site magnetic moments, of EMD and of M_s from the comparative study of Frank–Kasper-like environments shows that this approach can provide adequate guidance in the search for better rare-earth–transition-metal (TM = Fe, Co) permanent magnets.

[3] Author to whom any correspondence should be addressed.

0953-8984/03/467953+27$30.00

1. Introduction

Among the recently discovered hard-magnetic Fe-rich compounds, with intrinsic properties that are relevant for applications in rare-earth (R)–3d-transition-metal (Fe, Co) permanent magnets (RTPMs), are [1] ternary alloys with the $ThMn_{12}$-type structure (1:12) and interstitially modified [2, 3] $R_2Fe_{17}X$ (2:17) and $R_3(Fe, TM)_{29}X$ (3:29) compounds [4] (TM = transition metal, X = N, C, H). The introduction of N, or H, or C in the aforementioned intermetallics [1, 2, 4] by applying the gas–solid reaction has been proved a major advancement in this direction. These interstitially modified compounds alter substantially the anisotropy field (H_A), the ordering temperature (T_c) and the saturation magnetization (M_s) of the parent intermetallics by expanding their unit-cell volume to accommodate the absorbed elements without changing their crystal structure. Depending on the site occupancy, size and bonding of the interstitial element with its nearest neighbours (nns) a reduction or enhancement of each one of the three parameters can be obtained. However, simple models such as those based purely on the coordination number or on the average bond distance [5] are inadequate to provide theoretical guidance in the search for better RTPMs.

From the physical point of view, the influence of these interstitial elements on H_A and T_c can be explained in terms of crystal electric field (CEF) and molecular field approximations [6] at the R site for H_A and from the spin-fluctuation theory [6, 7] for the T_c. However, an estimation of M_s in RFe-rich intermetallics requires very accurate, first-principles, band structure calculations with sufficient predictive power to derive the local moments on each different Fe site. Furthermore, it is not always possible to compare the calculated moments with experimental values because a direct measurement of the magnitude of an Fe site magnetic moment μ^i_{Fe} is not always feasible for this complex class of magnets. Thus, although neutron diffraction and ^{57}Fe Mössbauer spectra can provide experimental samplings of moment values [9] when there are many inequivalent Fe sites, these techniques cannot always provide a suitable measure of individual site moments. So far, comparisons between experimental and calculated Fe moments, derived from *ab initio* band structure calculations, have shown [10] that site volumes appear to be important to the magnitude of a site magnetic moment.

The 3:29 phase offers a good case to study the dependence of local Fe moments on their environments within a single compound because it has a low crystal symmetry [11] that contains 11 distinct Fe sites of different local environments. This study investigates the topologies and the volumes of the Wigner–Seitz (WS) cells of individual Fe sites in $Nd_3(Fe, Ti)_{29}$ and $Nd_3(Fe, Ti)_{29}N_x$ intermetallics, taking advantage of the topological stability that is characteristic of the WS cell assignments in Frank–Kasper phases [12]. Earlier, Watson *et al* [13, 14] treated RTPMs as Frank–Kasper-like structures [12] with the TM atoms in 12-, 13- and 14-fold coordinated sites, and the R atoms typically in much larger 20-fold sites. The R sites are connected to each other and to the larger 3d sites by sixfold, $-72°$ disclination lines, a disclination being a rotational defect [15]. The orientations of the R-site crystal fields in RTPMs appear to be associated with the sixfold $-72°$ disclination lines of which a number pass through a site, defining *major* disclination lines when they involve some R–R nn pairs [13, 14]. Watson and Weinert [13] have used Frank–Kasper-like structures to understand the effect of site environments on the magnitude of individual Fe moments and on anisotropy axes in 1:5, 1:12 and 2:17 RTPM compounds, whereas Grandjean and Long [8] have used extensively a WS cell volume analysis for the assignment of ^{57}Fe Mössbauer spectral components to site environments in R_2Fe_{17} and $R_2Fe_{17}N_3$ compounds. Our aim is to extend their analysis in the $Nd_3(Fe, Ti)_{29}$ and $Nd_3(Fe, Ti)_{29}N_x$ types of structure and to investigate the correlations between individual Fe moments and six-edged facets (or disclination lines) in their WS cells.

2. Experimental details

The samples were prepared by arc-melting elemental constituents of high purity (99.9%) with the starting composition $Nd_3Fe_{27.5}Ti_{1.5}$, subsequently followed by annealing in vacuum at 1373 K for three days, wrapped in Ta foil and sealed in quartz tubes, and then quenching in water. The annealed samples were pulverized (grain sizes less than 37 μm) and the nitrides prepared with a gas–solid reaction, using high purity nitrogen gas at 4 atm for 12 h at 673 K. Dc magnetic measurements reveal a Curie temperature $T_c = 430(3)$ K for the $Nd_3Fe_{27.5}Ti_{1.5}$ compound and a $T_c = 710(3)$ K for the $Nd_3Fe_{27.5}Ti_{1.5}N_x$ nitride. Thus, the used temperature–pressure conditions correspond to a nitrogen concentration [16] $x \approx 4$. X-ray diffraction (XRD) spectra were collected at ambient conditions with a Siemens D500 diffractometer, using θ–2θ scans with Cu Kα_1 radiation. Neutron powder diffraction (NPD) measurements were performed at 295 K in the high-resolution powder diffractometer (HRPD) at the neutron spallation source ISIS, Rutherford Appleton Laboratory, United Kingdom. NPD spectra were collected from the backscattering data bank at $2\theta = 168.33°$ and the data were normalized and corrected for absorption. In each sample care was taken to account for the magnetic scattering from the Nd and Fe sublattices. To compare the parent and nitride structures we have chosen to collect the NPD spectra at room temperature because heating the samples to above their T_c values (to eliminate the magnetic scattering) could prove to be disadvantageous due to probable decomposition of the metastable 3:29 phase and, especially, of its nitride.

3. Rietveld refinement

3.1. Crystal structure refinement

As shown in [11], and confirmed in [17], the most accurate description of the 3:29 structure could be made by using the $A2/m$ space group instead of the [18, 19] $P2_1/c$. The initial assignment of the $A2/m$ space group was based, first, on extinction rules that are consistent with this choice, and second, on unacceptably high correlation coefficients when the $P2_1/c$ space group was used in the least-squares refinement of the structure [11]. However, in a recent study [20] it has been argued that only theoretical calculations can distinguish the tiny differences between the $A2/m$ and $P2_1/c$ space groups in the 3:29 structure. In this study, the refinement of the HRPD data shows unambiguously that the $P2_1/c$ space group does not provide the most accurate description of the structure because there are both high correlation coefficients between the symmetry related positional parameters and higher standard deviations for these parameters, which are two or three times larger than the corresponding parameters of symmetry independent atoms. Such features are common indications for a wrong assignment of a space group [21]. The high resolution of our NPD spectra shows definitely that all these problems are eliminated when the $A2/m$ space group is used.

The monoclinic $A2/m$ (No 12, cell choice 2) space group [11] has been applied as a starting model for the 3:29 structure. Figures 1 and 2 show the observed, calculated and difference NPD patterns for the $Nd_3(Fe, Ti)_{29}$ and the nitride compounds respectively. The vertical bars indicate the positions of the nuclear Bragg peaks for the three phases used. Table 1 lists the obtained structural parameters. Every second row in table 1 that is below a labelled atom in $Nd_3(Fe, Ti)_{29}$ contains the parameters for its nitride. In addition, there are two different notations for the Fe sites [11, 17] which are shown in the first column of table 1 (a single asterisk shows the labelling from [11] and a double asterisk shows the corresponding labels from [17]). To facilitate the comparison between the crystallographic data we adopt in this study the notation that is used in [17].

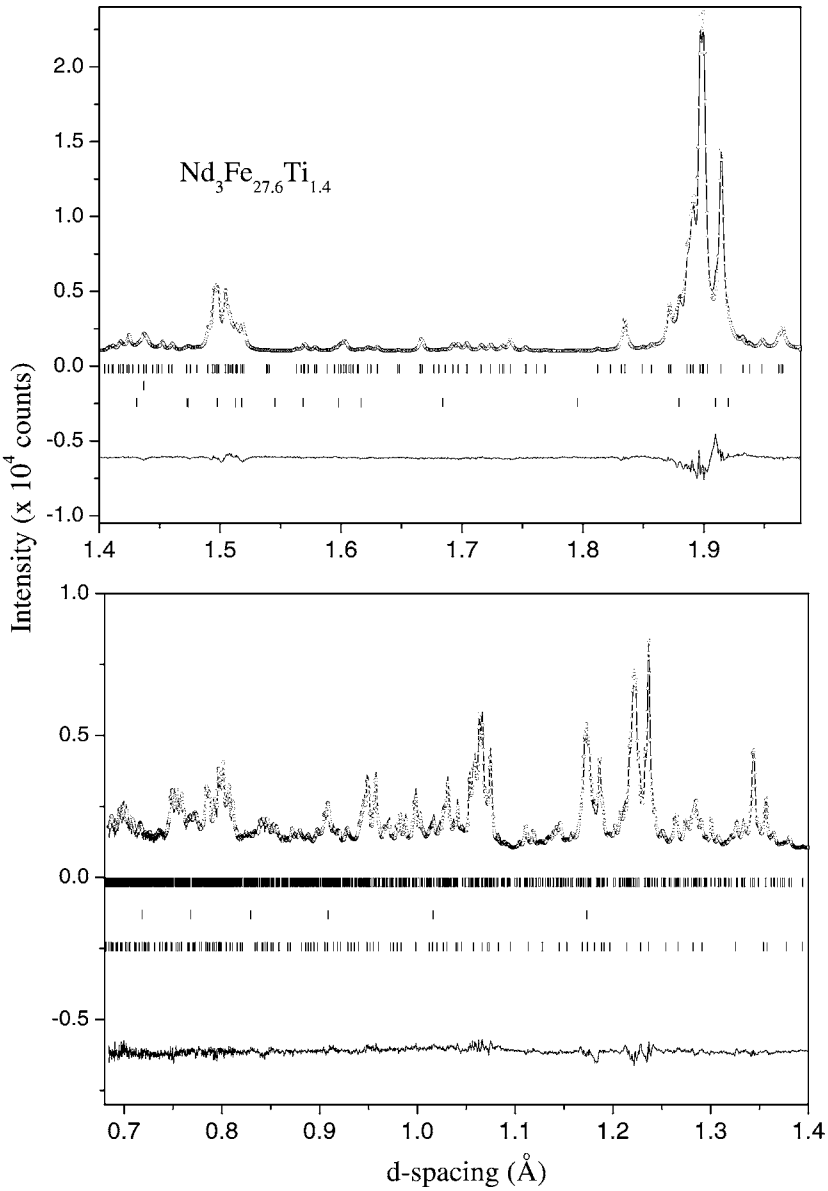

Figure 1. The observed, calculated and difference time-of-flight NPD patterns of $Nd_3Fe_{27.60(3)}Ti_{1.40(3)}$. Vertical bars indicate the position of nuclear Bragg peaks for the $Nd_3(Fe, Ti)_{29}$ type of structure, for α-Fe and for the $Nd(Fe, Ti)_{12}$ phase.

Since the examined high-resolution ($\Delta d/d \approx 10^{-3}$) region of the time of flight NPD spectra includes d-spacings between 0.6 and 2.3 Å, the contribution of magnetic intensity is negligibly small only for short d-spacing data due to the very rapid fall-off in the magnetic form factor. In HRPD, the magnetic scattering contributions for d-spacings less than 1.9 Å were found [22] to be entirely negligible in comparison with the nuclear scattering. Thus, the Rietveld refinement of the NPD data was performed with the Fullprof program [23] in two stages because a full-profile refinement structural analysis is further complicated by the presence of magnetic scattering for d-spacings between 1.9 and 2.3 Å.

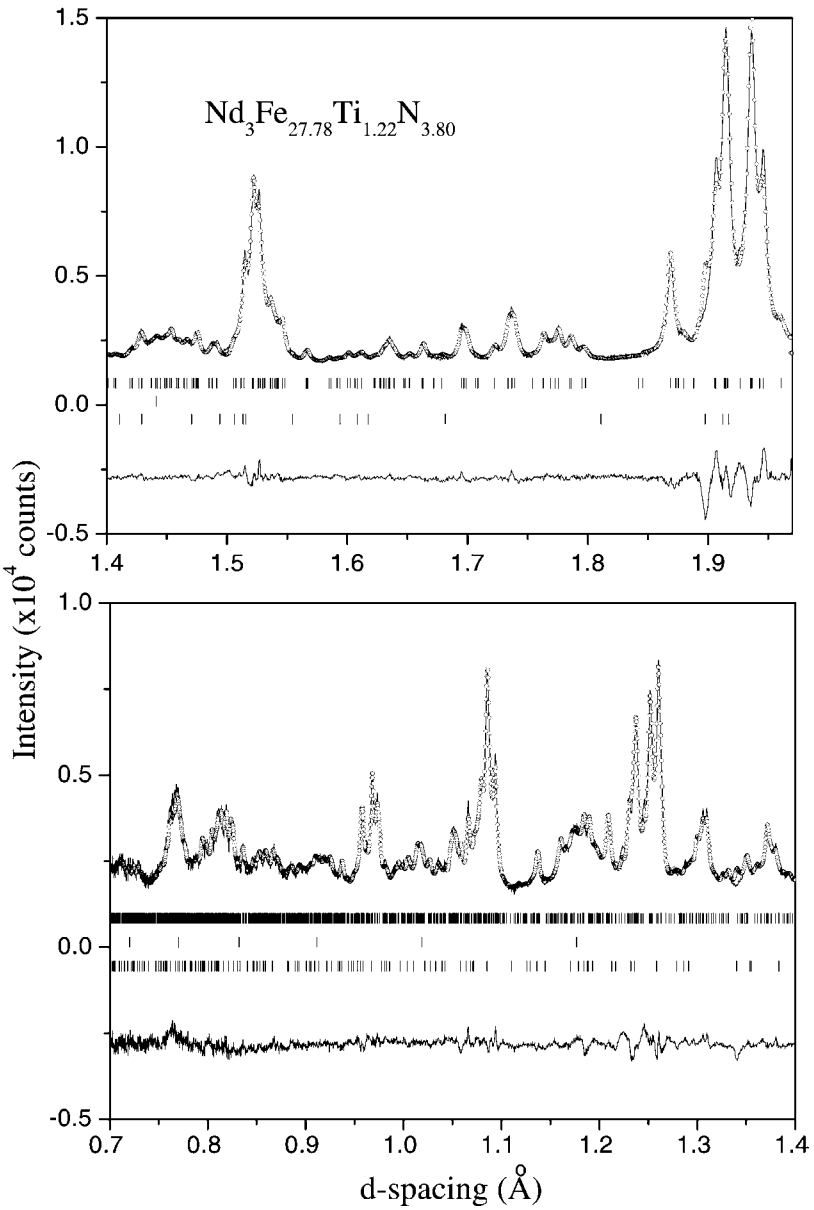

Figure 2. The observed, calculated and difference time-of-flight NPD patterns of $Nd_3Fe_{27.78(5)}Ti_{1.22(5)}N_{3.80(6)}$. Vertical bars indicate the position of nuclear Bragg peaks for the $Nd_3(Fe, Ti)_{29}$ type of structure, for α-Fe and for the $Nd(Fe, Ti)_{12}$ phase.

In the first stage, the structural refinement was performed only for the nuclear scattering [22] of the NPD spectrum, including d-spacings between 0.6 and 1.9 Å. Figures 1 and 2 show the structural refinements of the HRPD spectra and table 1 lists the best-fit structural parameters. The high resolution of the NPD data allows a quantitative estimation of the secondary phases, that coexist with the metastable 3:29 phase, together with the refinement of the structural parameters. Thus, a significant reduction of the reliability factors (R_B and R_w) is achieved when a minor 1:12 phase (space group $I4/mmm$) is used in addition to the

Table 1. Estimated crystallographic parameters for the $Nd_3Fe_{27.60(3)}Ti_{1.40(3)}$ and $Nd_3Fe_{27.78(5)}Ti_{1.22(5)}N_{3.80(6)}$ compounds from NPD data. Space group $A2/m$ (No 12, cell choice 2). Each parenthesis includes the estimated error in the last digit. Every second row underneath the labelled atoms corresponds to the same atom in the structure of the nitride. Exactly the same parameters fit very well the observed XRD spectra.

Atom	Site	x	y	z	B (Å^2)	Occupancy
Nd(1)[a], Nd_1[b]	2a	0.0	0.0	0.0	0.3(2)	1.0
Nitride	2a	0.0	0.0	0.0	0.24(6)	1.0
Nd(2)[a], Nd_2[b]	4i	0.5957(5)	0.0	0.1841(5)	0.4(1)	1.0
Nitride	4i	0.5934(6)	0.0	0.1831(7)	0.24(6)	1.0
Fe(1)[a], Fe_1[b]	2c	0.5	0.0	0.5	0.6(1)	1.0
Nitride	2c	0.5	0.0	0.5	0.88(2)	1.0
Fe(2)/Ti(2)[a], Fe_7[b]	4i	0.1386(7)	0.0	0.2917(7)	0.5(3)	0.76(2)/0.24(2)
Nitride	4i	0.1344(7)	0.0	0.2946(9)	0.88(2)	0.83(1)/0.17(1)
Fe(3)/Ti(3)[a], Fe_6[b]	4i	0.2545(8)	0.0	0.5255(8)	0.5(3)	0.70(2)/0.30(2)
Nitride	4i	0.2527(10)	0.0	0.5283(11)	0.88(2)	0.74(1)/0.26(1)
Fe(4)[a], Fe_9[b]	8j	0.8019(4)	0.7843(3)	0.0912(4)	0.69(5)	1.0
Nitride	8j	0.8018(5)	0.7797(4)	0.0903(6)	0.88(2)	1.0
Fe(5)[a], Fe_8[b]	8j	0.6259(3)	0.6458(4)	0.1849(4)	0.49(6)	1.0
Nitride	8j	0.6319(5)	0.6400(6)	0.1821(6)	0.88(2)	1.0
Fe(6)/Ti(6)[a], Fe_3[b]	4g	0.0	0.3577(7)	0.0	0.4(2)	0.84(2)/0.16(2)
Nitride	4g	0.0	0.3587(9)	0.0	0.88(2)	0.82(2)/0.18(2)
Fe(7)[a], Fe_4[b]	4i	0.8930(4)	0.0	0.2790(6)	0.72(9)	1.0
Nitride	4i	0.8908(7)	0.0	0.2798(8)	0.88(2)	1.0
Fe(8)[a], Fe_{11}[b]	8j	0.8000(3)	0.2457(6)	0.3426(4)	0.46(5)	1.0
Nitride	8j	0.8016(5)	0.2496(8)	0.3460(6)	0.88(2)	1.0
Fe(9)[a], Fe_5[b]	4i	0.7102(2)	0.0	0.9080(6)	0.50(7)	1.0
Nitride	4i	0.7151(7)	0.0	0.9078(8)	0.88(2)	1.0
Fe(10)[a], Fe_{10}[b]	8j	0.4049(3)	0.7495(4)	0.0645(3)	0.44(7)	1.0
Nitride	8j	0.4035(4)	0.7418(5)	0.0678(5)	0.88(2)	1.0
Fe(11)[a], Fe_2[b]	4e	0.0	0.25	0.25	0.44(9)	1.0
Nitride	4e	0.0	0.25	0.25	0.54(2)	1.0
N(1)	4f	0.5	0.25	0.75	0.54(6)	1.00(2)
N(2)	4i	0.2046(8)	0.0	0.9052(8)	0.54(6)	0.90(2)

[a] Notation after [11].
[b] Notation after [17].

major 3:29 phase, whereas all samples contain traces of α-Fe. The estimated stoichiometry is $Nd_3Fe_{27.60(3)}Ti_{1.40(3)}$, the unit cell dimensions are $a = 10.6459(1)$ Å, $b = 8.5942(1)$ Å, $c = 9.7517(1)$ Å and $\beta = 96.938(1)^\circ$ and the volume $V = 885.68(2)$ Å^3. The reliability factors are $R_p = 4.15\%$, $R_{wp} = 4.99\%$, $R_{exp} = 2.01\%$ and $\chi^2 = 6.12$. The R_B factors are 5.65% for the 3:29 phase, 4.77% for α-Fe and 8.18% for the 1:12 phase. The sample contains 84.2% of 3:29, 4.4% of α-Fe and 11.4% of 1:12. For the nitride the estimated stoichiometry is $Nd_3Fe_{27.78(5)}Ti_{1.22(5)}N_{3.80(6)}$, which is consistent with the obtained relative unit cell volume expansion of 5.35%. In addition, a nitrogen concentration of 3.80(6) atoms/fu is close to the theoretically expected value of four for maximum nitrogen uptake. The corresponding unit cell dimensions of the nitride are $a = 10.8781(3)$ Å, $b = 8.7471(2)$ Å, $c = 9.8896(4)$ Å and $\beta = 97.371(3)^\circ$, and volume $V = 933.24(5)$ Å^3. The reliability factors are $R_p = 3.88\%$, $R_{wp} = 4.88\%$, $R_{exp} = 2.05\%$ and $\chi^2 = 5.67$. The R_B factors are 4.28% for the 3:29 phase, 2.89% for α-Fe and 11.00% for the 1:12 phase. The nitride contains 83% of 3:29, 10% of α-Fe and 7% of 1:12.

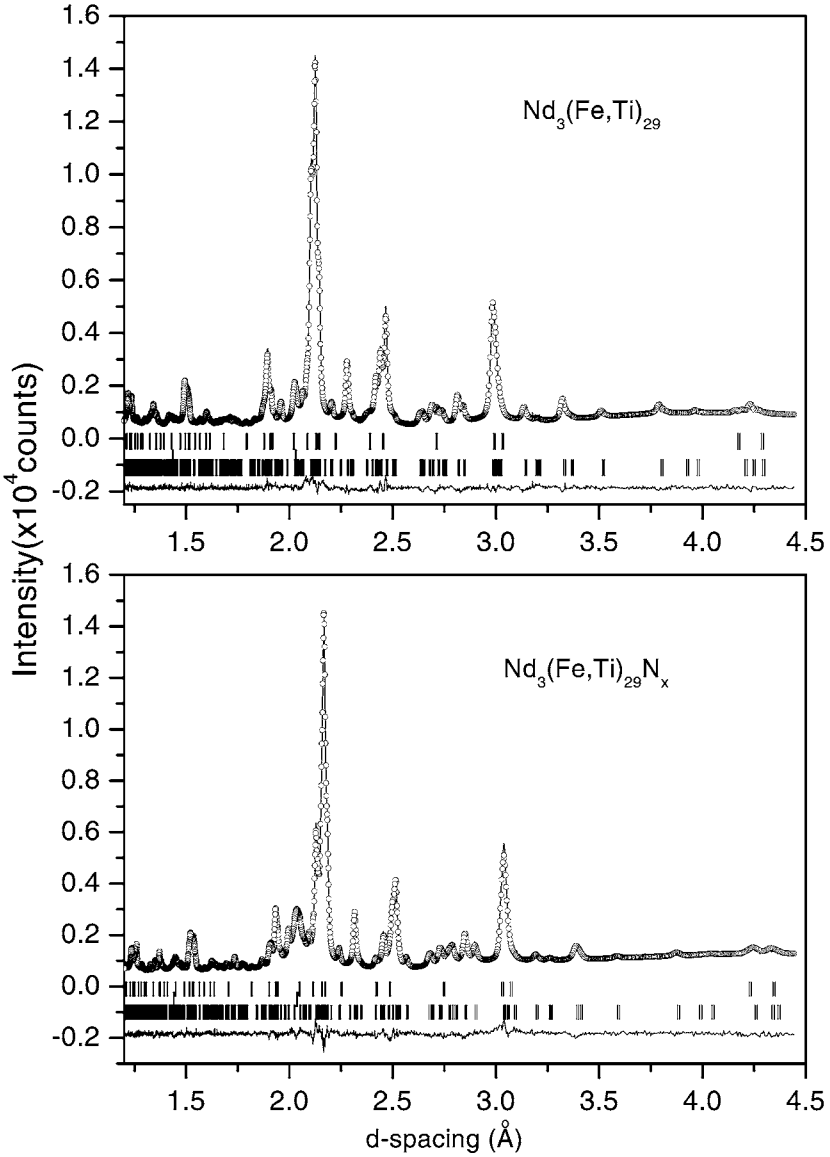

Figure 3. The observed, calculated and difference XRD patterns of $Nd_3Fe_{27.60(3)}Ti_{1.40(3)}$ (top) and $Nd_3Fe_{27.78(5)}Ti_{1.22(5)}N_{3.80(6)}$ (bottom). Vertical bars indicate the position of nuclear Bragg peaks for the $Nd_3(Fe, Ti)_{29}$ type of structure, for α-Fe and for the $Nd(Fe, Ti)_{12}$ phase.

Note that the concentration of Ti changes from 1.40 atoms/fu in $Nd_3Fe_{27.60(3)}Ti_{1.40(3)}$ to 1.22 in $Nd_3Fe_{27.78(5)}Ti_{1.22(5)}N_{3.80(6)}$. These results are, generally, in agreement with those obtained [17, 24] in $Nd_3(Fe, Ti)_{29}$ compounds where a 40% reduction of Ti was reported [24] upon nitrogen uptake as well. In comparison, 1:12 compounds with V or Ti stabilizing elements follow a similar trend [25] because this phase decomposes to a certain degree during the nitrogenation process into α-Fe and an amorphous phase. Thus, such effects can explain the obtained change ($\approx$13%) of the Ti content upon nitrogen uptake in the 3:29 structure.

Figure 3 shows the observed, calculated and difference XRD profiles that were calculated using the structural parameters from table 1. The obtained reliability factors for the parent (nitride) XRD spectra are $R_p = 4.66\%$ (4.81%), $R_{wp} = 6.75\%$ (5.92%) and $R_{exp} = 3.12\%$ (2.77%). The R_B factor for the parent (nitride) 3:29 phase is 5.39% (5.02%). Remarkably, figures 1–3 show that exactly the same structural parameters (from table 1) fit very well both the observed XRD and NPD spectra. The excellent agreement between the observed and calculated XRD spectra with the structural parameters of table 1 indicates that the contribution of magnetic scattering is very small in the data range used for the NPD refinement, and thus it does not influence the structural parameters. It is worth noting that, generally, neutron HRPD data can provide more accurate (high-precision) crystal structure parameters than XRD data because the nuclear scattering factor b_o is isotropic (does not depend on $\sin\theta/\lambda$). Thus nuclear scattering decreases only because of the temperature effect and Bragg reflections can be collected at very short d-spacings, giving atomic positions and thermal parameters with accuracy higher than from x-rays. In addition, the neutron scattering lengths vary non-monotonically with the atomic number Z and thus it is possible to localize the positions between atoms having very close values of Z (in our case, between Fe and Ti atoms). These two properties are indicative of the necessity of neutron HRPD measurements in our case, whereas the excellent fit of the XRD profiles with the derived parameters from NPD data *shows the credibility* of the crystal structure analysis.

3.2. Magnetic refinement

In the second stage, the crystal structure parameters from table 1 were used as starting parameters for the refinement of the entire NPD spectrum (d-spacings between 0.6 and 2.3 Å) including both nuclear and magnetic intensities. Since the HRPD data contain magnetic scattering contributions that arise from the decaying part of the magnetic form factors ($f_{Nd^{3+}}$ and metallic f_{Fe}) and the strongest magnetic reflections (for d-spacings greater than 2.3 Å) could not be recorded in this type of experiment, this second stage of refinement examines mainly the effect of magnetic contributions on the structural parameters determined in the first stage (table 1). Because of the large number of Fe sites (monoclinic symmetry) and the missing peaks for d-spacings greater than 2.3 Å, the magnetic scattering was modelled assuming all the moments were collinear. In addition, the Fe moments were constrained to be equal in magnitude, as were the Nd moments, and the two sublattice moments were allowed to refine indepedently. At this stage, all the structural parameters were allowed to refine, without any constraint, together with the magnetic moments of Fe and Nd atoms. A summary of the calculated magnetic scattering profiles is given in figure 4, where the observed and calculated profiles are given in the region between 1.9 and 2.3 Å for clarity. Four cases were studied thoroughly and the results are the following.

(i) *The direction of magnetic moments parallel to the a-axis of the crystal structure, as suggested in* [24]. The derived magnitudes of magnetic moments for the parent compound are $\mu_{Fe} = 1.9(1)\ \mu_B$ and $\mu_{Nd} = 3.3(2)\ \mu_B$ and the reliability factors are $R_{wp} = 5.39\%$, $R_B = 4.93\%$ for the 3:29 phase and $R_M = 4.68\%$. The derived magnitudes of magnetic moments for the nitride are $\mu_{Fe} = 2.2(1)\ \mu_B$ and $\mu_{Nd} = 3.1(2)\ \mu_B$ and the reliability factors are $R_{wp} = 5.11\%$, $R_B = 5.24\%$ for the 3:29 phase and $R_M = 5.44\%$. Figure 4 shows the calculated profiles, and the difference pattern (bottom curve) between the observed and total calculated profiles is given only for this case.

(ii) *The direction of magnetic moments parallel to the* $[20\bar{1}]$ *direction of the crystal structure, as suggested in* [26, 27]. The derived magnitudes of magnetic moments for the parent compound are $\mu_{Fe} = 1.8(1)\ \mu_B$ and $\mu_{Nd} = 3.3(2)\ \mu_B$ and the reliability factors are

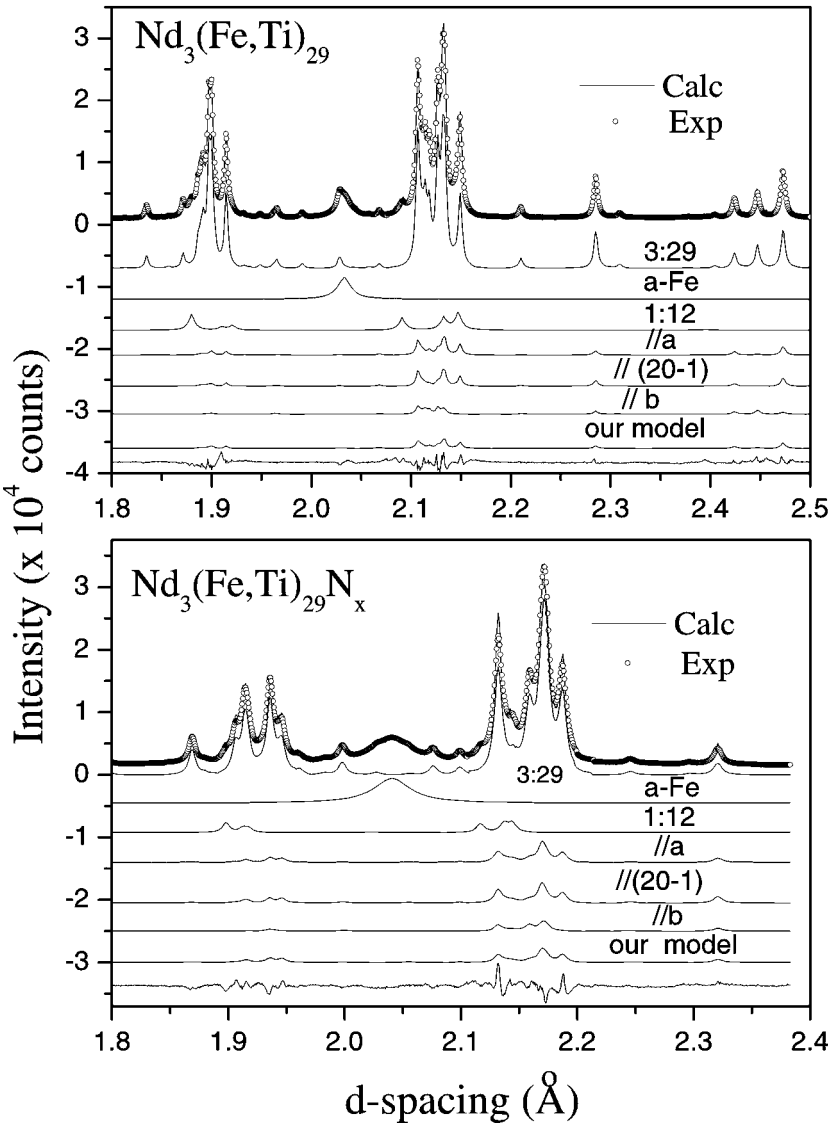

Figure 4. The observed, calculated total profile, calculated nuclear and magnetic sub-spectra and the difference (lower line) time-of-flight NPD patterns of $Nd_3Fe_{27.60(3)}Ti_{1.40(3)}$ (top) and $Nd_3Fe_{27.78(5)}Ti_{1.22(5)}N_{3.80(6)}$ (bottom). The difference pattern is between the observed and the total calculated profile when the magnetic moments are aligned parallel to the a-axis (see the text).

$R_{wp} = 5.39\%$, $R_B = 4.97\%$ for the 3:29 phase and $R_M = 4.99\%$. The derived magnitudes of magnetic moments for the nitride are $\mu_{Fe} = 2.3(1)\ \mu_B$ and $\mu_{Nd} = 2.9(2)\ \mu_B$ and the reliability factors are $R_{wp} = 5.07\%$, $R_B = 4.97\%$ for the 3:29 phase and $R_M = 5.61\%$. Figure 4 shows the calculated profile.

(iii) *The direction of magnetic moments parallel to the b-axis of the crystal structure*. The derived magnitudes of magnetic moments for the parent compound are $\mu_{Fe} = 1.1(1)\ \mu_B$ and $\mu_{Nd} = 3.3(2)\ \mu_B$ and the reliability factors are $R_{wp} = 5.66\%$, $R_B = 5.88\%$ for the

3:29 phase and $R_M = 7.33\%$. The derived magnitudes of magnetic moments for the nitride are $\mu_{Fe} = 1.3(1)\ \mu_B$ and $\mu_{Nd} = 3.0(2)\ \mu_B$ and the reliability factors are $R_{wp} = 5.17\%$, $R_B = 5.05\%$ for the 3:29 phase and $R_M = 7.15\%$. Figure 4 shows the calculated profile.

(iv) *The direction of magnetic moments parallel to the* $[20\bar{1}]$ *direction of the crystal structure and the magnitudes of individual* μ^i_{Fe} *values taken from table* 4 (*see section* 5) *for the parent and the nitride compounds.* The magnetic moments for the Nd sites have been kept fixed at $\mu_{Nd} = 2.2\ \mu_B$. Only the structural parameters were allowed to refine. The reliability factors for the parent profile are $R_{wp} = 5.43\%$, $R_B = 5.09\%$ for the 3:29 phase and $R_M = 5.67\%$. The reliability factors for the nitride are $R_{wp} = 5.12\%$, $R_B = 5.20\%$ for the 3:29 phase and $R_M = 5.59\%$. Figure 4 shows the simulated profile for this case. The purpose of this simulation is to show that the magnetic configuration in section 5 is, first, compatible with the NPD refinement and, second, equivalent with the test cases of $\mu_{Fe} \parallel \mu_{Nd} \parallel a$-axis and $\mu_{Fe} \parallel \mu_{Nd} \parallel [20\bar{1}]$-direction.

Note that the highest mismatch appears between the calculated and experimental profiles of the nitride (figures 2 and 4) in stage-one and stage-two refinements. As seen in figure 4, these differences cannot be explained from the contribution of magnetic scattering. Thus, it can be argued that anisotropic peak broadening, due to size and/or strain effects, is responsible for these differences.

The main result of this stage-two refinement is that the derived structural parameters do not deviate from the values given in table 1 (deviations are within the error shown at the last digit) for these four magnetic configurations. This shows clearly that, for the specific data range of the HRPD instrument, *the magnetic scattering does not affect the structural parameters* derived from stage-one refinement. A comparison of magnetic moments and reliability factors shows that the third case (parallel to the b-axis) is most unlikely to occur because the derived μ_{Fe} values are very small and the R_M is the highest among the R-factors of the three other cases. This indicates that the major component of the average magnetic vector is lying in a plane perpendicular to b-axis before and after nitrogen uptake. Note that, although we have scanned all the space by constraining the direction of magnetic moments within the (010) plane (vertical to the b-axis) of the crystal structure, the results are inconclusive for a specific moment direction within the (010) plane because the obtained R_M values are slightly different from each other, as in cases (i) and (ii) above. In addition, figure 4 shows that the mismatch of intensities in the difference pattern is comparable with the calculated magnetic intensities for the four cases examined. These results show that the experimental data, collected from the HRPD instrument, are not adequate to solve the magnetic structure of 3:29. However, the solution of the magnetic structure is beyond the scope of the present study and more suitable neutron scattering experiments, such as spin-polarized spectra, are required for this purpose.

4. Radical construct of Wigner–Seitz cells

A procedure known as the *radical construct* of WS cells is used [13, 14] to determine the local environment of the Fe sites. The program [28] DIDO95 was used for the construction of volume filling cells. The scheme involves assigning spheres, with radii reflecting assigned sizes, to the different atoms. Specifically, atomic radii of 1.26, 1.82, 1.47 and 0.92 Å were assigned for Fe, Nd, Ti and N atoms respectively. An average radius has been assigned for statistically occupied sites by Fe and Ti atoms. These values are 1.294, 1.323 and 1.310 Å for the Fe_3, Fe_6 and Fe_7 sites in $Nd_3(Fe, Ti)_{29}$ and 1.298, 1.315 and 1.296 Å for the corresponding sites in the nitride (see table 1). The calculated WS cell volumes of the parent and the nitride 3:29 compounds are listed in the fifth column of table 2.

Table 2. WS cell polyhedra, volumes, nns, Fe occupancies and average atomic distances calculated for the $Nd_3(Fe, Ti)_{29}$ and the nitride compounds. For the notation see the text. Every second row underneath the labelled atoms corresponds to the same atom in the structure of the nitride.

Group	Atom	Site	Polyhedron	Volume (Å^3)	[N_t, N_R, N_{TM}, N_N]	Fe in nn sites	$\langle r \rangle$ (Å)
	Nd_1	2a	(0, 0, 12, 8)	30.63	[20, 0, 20, 0]	19.20	3.144
	Nitride	2a	(0, 2, 8, 12)	30.86	[22, 0, 20, 2]	19.30	3.192
	Nd_2	4i	(0, 0, 12, 8)	31.63	[20, 1, 19, 0]	18.70	3.168
	Nitride	4i	(0, 3, 6, 14)	31.92	[23, 1, 19, 3]	18.70	3.252
A	Fe_1	2c	(0, 0, 12, 0)	11.44	[12, 2, 10, 0]	9.40	2.507
A	Nitride	2c	(0, 0, 12, 0)	11.88	[12, 2, 10, 0]	9.48	2.563
A	Fe_2	4e	(0, 0, 12, 0)	11.27	[12, 2, 10, 0]	9.20	2.513
A	Nitride	4e	(0, 0, 12, 0)	11.92	[12, 2, 10, 0]	9.30	2.558
A	Fe_{11}	8j	(0, 0, 12, 0)	11.24	[12, 2, 10, 0]	9.30	2.504
A	Nitride	8j	(0, 0, 12, 0)	11.82	[12, 2, 10, 0]	9.39	2.542
B	Fe_4	4i	(0, 0, 12, 0)	11.65	[12, 2, 10, 0]	9.14	2.566
B	Nitride	4i	(0, 1, 10, 2)	11.80	[13, 2, 10, 1]	9.21	2.616
B	Fe_8	8j	(0, 0, 12, 0)	11.92	[12, 2, 10, 0]	9.46	2.598
	or		(0, 1, 10, 2)	11.91	[13, 2, 11, 0]		
B	Nitride	8j	(0, 1, 10, 2)	11.81	[13, 2, 10, 1]	9.57	2.625
B	Fe_9	8j	(0, 0, 12, 0)	11.78	[12, 2, 10, 0]	9.30	2.594
	or		(0, 1, 10, 2)	11.78	[13, 2, 11, 0]		
B	Nitride	8j	(0, 1, 10, 2)	11.77	[13, 2, 10, 1]	9.39	2.652
C	Fe_5	4i	(0, 0, 12, 0)	12.03	[12, 3, 9, 0]	8.76	2.576
C	Nitride	4i	(0, 1, 10, 2)	12.23	[13, 3, 9, 1]	8.83	2.626
C	Fe_{10}	8j	(0, 0, 12, 0)	12.03	[12, 3, 9, 0]	8.70	2.563
C	Nitride	8j	(0, 1, 10, 2)	12.33	[13, 3, 9, 1]	8.74	2.622
D	Fe_3	4g	(0, 0, 12, 2)	13.04	[14, 1, 13, 0]	11.76	2.712
D	Nitride	4g	(0, 0, 12, 2)	13.63	[14, 1, 13, 0]	11.90	2.757
D	Fe_6	4i	(0, 0, 12, 2)	13.57	[14, 1, 13, 0]	12.44	2.713
D	Nitride	4i	(0, 0, 12, 2)	13.89	[14, 1, 13, 0]	12.47	2.738
D	Fe_7	4i	(0, 0, 12, 2)	13.26	[14, 1, 13, 0]	12.38	2.706
D	Nitride	4i	(0, 0, 12, 2)	13.57	[14, 1, 13, 0]	12.38	2.736
	N(1)	4f	(0, 6, 0, 0)	3.81	[6, 2, 4, 0]		
	N(2)	4i	(0, 6, 0, 0)	3.69	[6, 2, 4, 0]		

It will be instructive for the following to provide a brief description of some Frank–Kasper environments. Frank–Kasper-like structures are stable in the number and arrangement of facets over chemically reasonable ranges of choices of radii. Usually, the 3d atoms are in Frank–Kasper WS cells which are predominantly made up of five-edged facets, with some cells having a few six-edged facets [13]. The notation $(a, b, c, \ldots)$ indicates a cell having a three-edged, b four-edged, c five-edged, ... facets. The number of edges on a facet indicates how many nns are common to the nn pair responsible for the facet. Frank–Kasper Fe environments involve 12-, 14-, 15- and 16-fold [13] numbers of atomic nns. The 12- and 14-fold environments involve 12 nns which share five common nns along the bond line to the central atom, contributing 12 five-edged facets to the WS cells. The 14-fold environments involve, in addition, two nns which share six common nns with the centre atoms, thus contributing two six-edged facets to the WS cells [29]. Nelson [15] called $-72°$ disclinations the sixfold bond lines. Thus, the building blocks involve zero, two, three or four sixfold bond lines or $-72°$ disclinations. To be more explicit, the (0, 0, 12, 2) has two bond lines lying approximately in a straight line; the

(0, 0, 12, 3) has the three bond lines 120° away from each other in a plane and the (0, 0, 12, 4) has them arranged tetrahedrally, whereas a (0, 0, 12, 1) WS cell is topologically impossible.

Using structural parameters from the Rietveld refinement (table 1) all the related parameters with WS polyhedra were calculated for every site in $Nd_3(Fe, Ti)_{29}$ and $Nd_3(Fe, Ti)_{29}N_x$ (table 2). The last three columns in table 2 list from left to right the number of nns in every cell, using the notation $[N_t, N_R, N_{TM}, N_N]$ with N_t = (total number of nns), N_R = (number of R nns), N_{TM} = (number of TM nns), N_N = (number of N nns) and $N_t = N_R + N_{TM} + N_N$; the atomic occupancy of the TM nn sites in Fe and the average atomic distance in every cell $\langle r \rangle$. The fourth column in table 2 lists the WS polyhedra (a, b, c, d) for every site in $Nd_3(Fe, Ti)_{29}$ and its nitride. A first inspection of table 2 reveals that some of the 12-fold Fe environments in $Nd_3(Fe, Ti)_{29}$ transform to 13-fold environments upon nitrogen uptake, following the Frank–Kasper sequence (0, 0, 12, 0) → (0, 1, 10, 2), whereas all the 14-fold (0, 0, 12, 2) TM environments remain intact upon nitrogenation. In addition, table 2 shows that the Fe_8 and Fe_9 sites adopt a 13-fold (0, 1, 12, 2) environment before and after nitrogen uptake.

To identify some trends on μ^i_{Fe} and magnetic anisotropy as a function of WS cell characteristics it is necessary to make comparisons with the two closest relatives of the 3:29 structure, that are the 2:17R (2:17R is the rhombohedral Th_2Zn_{17} type of structure) and 1:12 (the tetragonal $ThMn_{12}$-type) structures [26] (3:29 = 1:12 + 2:17). Using data for the unit cell parameters from the literature [30–32] we have reproduced the polyhedra and the WS volumes for every site in Nd_2Fe_{17}, $Nd_2Fe_{16.3}Ti_{0.7}$ and their nitrides (table 3). For the *radical construct* of WS cells in $Nd_2Fe_{16.3}Ti_{0.7}$, an average radius of 1.33 Å has been assigned for the statistically occupied [30] Fe_1 (6c) site by 66% Fe (radius 1.26 Å) and 34% Ti (radius 1.47 Å). A comparison between Nd_2Fe_{17} and $Nd_2Fe_{16.3}Ti_{0.7}$ data in table 3 reveals that Ti substitution causes a relatively larger volume expansion of the WS cell in the 14-fold Fe_1 (6c) site that is occupied preferentially. The Fe_3 18f site has the 13-fold (0, 1, 10, 2) environment in the 2:17R structure. In addition, table 3 shows that Fe_3 remains in the 13-fold environment whereas the 12-fold environment of Fe_4 transforms to the 13-fold environment upon nitrogen uptake, following the sequence (0, 0, 12, 0) → (0, 1, 10, 2). The 14-fold (0, 0, 12, 2) environment in the Fe_1 site remains intact upon nitrogen uptake, as in the corresponding 3:29 sites.

Thus, using only the criterion of WS cell polyhedra, we can conclude that the 14-fold Fe_1 (6c-site) environment in the 2:17R structure has the same environment as the three 14-fold Fe_3 (4g), Fe_6 (4i) and F_7 (4i) sites (table 2) in the 3:29 structure. The 12-fold Fe_2 environment (9d site) in the 2:17R structure, that does not transform upon nitrogen uptake, shares the same topological stability with the three 12-fold Fe_1 (2c), Fe_2 (4e) and F_{11} (8j) sites (table 2) in the 3:29 structure. Finally, the 13- and 12-fold environments of 18f and 18h sites in the 2:17R structure respectively are expected to be the same as the environments of the five Fe_4 (4i), Fe_8 (8j), F_9 (8j), F_5 (4i) and F_{10} (8j) sites (table 2) in the 3:29 structure, that transform accordingly upon nitrogen uptake. However, these five Fe sites have different numbers of TM *nns* (table 2) and therefore should exhibit different μ^i_{Fe} values.

Based on WS cell construction data from tables 1 and 2 the nn environments for the 11 TM and two R sites of 3:29 are plotted in figures 5–10 together with the corresponding 2:17R (table 3) and 1:12 environments. Figure 5 shows the atomic arrangement of nns around the two inequivalent R sites (2a and 4i) in 3:29, the 6c R site in 2:17R, that shares the same environment as the 3:29 4i site, and the 2a R site in 1:12, that shares the same environment as the 3:29 2a site. In addition, table 3 shows that the 20-fold Nd environment (6c site) in 2:17R structure transforms to a non-Frank–Kasper cell upon nitrogen uptake: (0, 0, 12, 8) → (0, 3, 6, 14), as the Nd_2 (4i-site) environment in the 3:29 structure (table 2). Figures 6–10 reveal that the 11 iron sites in the 3:29 structure can be separated into four different categories of TM

Table 3. WS cell polyhedra, volumes, nns, average atomic distances and Fe occupancies calculated for Nd_2Fe_{17}, $Nd_2(Fe, Ti)_{17}$ and their nitrides. For the notation see the text. Every second row underneath the labelled atoms corresponds to the same atom in the structure of the nitride. The experimental data were taken from [30–32].

Compound	Atom	Site	Polyhedron	Volume (Å^3)	[N_t, N_R, N_{TM}, N_N]	$\langle r \rangle$ (Å)	Fe occupancies
Nd_2Fe_{17}	Nd	6c	(0, 0, 12, 8)	31.74	[20, 1, 19, 0]	3.169	
	Nitride	6c	(0, 3, 6, 14)	32.09	[23, 1, 19, 3]	3.249	
	Fe_1	6c	(0, 0, 12, 2)	12.29	[14, 1, 13, 0]	2.662	
	Nitride	6c	(0, 0, 12, 0)	12.76	[14, 1, 13, 0]	2.688	
	Fe_2	9d	(0, 0, 12, 0)	11.25	[12, 2, 10, 0]	2.448	
	Nitride	9d	(0, 0, 12, 0)	11.84	[12, 2, 10, 0]	2.526	
	Fe_3	18f	(0, 0, 12, 0)	11.79	[12, 2, 10, 0]	2.570	
	or		(0, 1, 10, 2)	11.73	[13, 2, 11, 0]		
	Nitride	18f	(0, 1, 10, 2)	11.74	[13, 2, 10, 1]	2.605	
	Fe_4	18h	(0, 0, 12, 0)	12.09	[12, 3, 9, 0]	2.563	
	Nitride	18h	(0, 1, 10, 2)	12.43	[12, 3, 9, 1]	2.627	
	N	9e	(0, 6, 0, 0)	3.75	[6, 2, 4, 0]		
$Nd_2Fe_{16.3}Ti_{0.7}$	Nd	6c	(0, 0, 12, 8)	31.56	[20, 1, 19, 0]	3.168	18.661
	Nitride	6c	(0, 3, 6, 14)	32.09	[23, 1, 19, 3]	3.238	
	Fe_1	6c	(0, 0, 12, 2)	13.65	[14, 1, 13, 0]	2.704	12.661
	Nitride	6c	(0, 0, 12, 0)	13.76	[14, 1, 13, 0]	2.698	
	Fe_2	9d	(0, 0, 12, 0)	11.28	[12, 2, 10, 0]	2.498	9.332
	Nitride	9d	(0, 0, 12, 0)	11.92	[12, 2, 10, 0]	2.533	
	Fe_3	18f	(0, 0, 12, 0)	11.90	[12, 2, 10, 0]	2.599	9.332
	or		(0, 1, 10, 2)	11.88	[13, 2, 11, 0]		
	Nitride	18f	(0, 1, 10, 2)	11.86	[13, 2, 10, 1]	2.607	
	Fe_4	18h	(0, 0, 12, 0)	11.98	[12, 3, 9, 0]	2.557	8.661
	Nitride	18h	(0, 1, 10, 2)	12.61	[12, 3, 9, 1]	2.626	
	N	9e	(0, 6, 0, 0)	3.75	[6, 2, 4, 0]		

environments, according to their WS cell polyhedra. The necessity of this grouping in the 3:29 structure emerged much earlier, during the analysis of one of the first ^{57}Fe Mössbauer spectra [33]. According to our WS cell treatment this grouping of the 11 iron sites in 3:29 compounds provides a deeper understanding of the site symmetries that is used in the next section to predict their intrinsic magnetic properties. The special features of each group are summarized below.

Group A includes Fe_1-2c [Fe(1)], Fe_2-4e [Fe(11)] and Fe_{11}-8j [Fe(8)] sites, with the same environment as the 9d site in the 2:17R structure (ten TM nns). A comparison of WS cell volumes (tables 2 and 3) shows similar values as well. In addition, their 12-fold environments (0, 0, 12, 0) remain intact upon nitrogen uptake (tables 2 and 3). Figure 6 shows the atomic arrangement of nns around the group-A sites, the 9d site in 2:17R and the 1:12 8f site, that shares a similar (0, 0, 12, 0) environment [34] with group-A sites as well.

Group B includes Fe_4-4i [Fe(7)], Fe_8-8j [Fe(5)] and Fe_9-8j [Fe(4)] sites, corresponding to the 18f site of 2:17R and to the 8f site of 1:12. The characteristic feature of group-B sites is the appearance of the 13-fold (0, 1, 10, 2) environment. Figure 7 shows that it can be constructed if one takes an (0, 0, 12, 0) environment and brings an extra atom in between several of the existing neighbours such that a pair of corners connected by a common edge of the WS cell is cut out and replaced by a new four-edged facet. In the (0, 1, 10, 2) cell, the single fourfold facet has the two sixfold facets as neighbours on opposite edges (figure 5). These short-ranged fourfold +72° disclination lines that begin and end at these types of site are called *minor* disclinations.

Table 4. Tentative assignment of site hyperfine fields B^i_{hf} at room temperature, site magnetic moments $\mu^i_{Fe} = B^i_{hf}/A_{hf}$ (an $A_{hf} = 17\ T/\mu_B$ was used only for the 1:12 nitrides[a] whereas for the rest it was $15\ T/\mu_B$) and saturation magnetizations per formula unit $M_s(Fe) = 27.3(\sum \mu^i_{Fe})/11$ for $Nd_3Fe_{27.3}Ti_{1.7}(\equiv Nd_2Fe_{16.3}Ti_{0.7} + NdFe_{11}Ti)$. Every second row underneath the labelled atoms corresponds to the same atom in the structure of the nitride. Each parenthesis next to atom labels shows the assignment from the corresponding 1:12 or 2:17R sites; mixed means the average value from the two corresponding 1:12 or 2:17R sites.

Structure	Atom	Site	B^i_{hf} (T)	μ^i_{Fe} (μ_B)	M_s(Fe) (μ_B/fu)
$NdFe_{11}Ti$[a]		8i	28.9	1.93	16.6
	Nitride	8i	34.4	2.02	20
	Fe	8f	19.9	1.33	
	Nitride	8f	27.2	1.6	
	Fe	8j	20.5	1.37	
	Nitride	8j	32.1	1.88	
$Nd_2Fe_{16.3}Ti_{0.7}$[b]	Fe_1	6c	22.3	1.49	12.9
	Nitride	6c	32.5	2.17	19.3
	Fe_2	9d	21.3	1.42	
	Nitride	9d	33.6	2.24	
	Fe_3	18f	19.1	1.28	
	Nitride	18f	25.7	1.72	
	Fe_4	18h	17.8	1.19	
	Nitride	18h	29.3	1.95	
$Nd_3Fe_{27.3}Ti_{1.7}$	Fe_1(9*d*/2:17)	2c	21.3	1.42	42.6
	Nitride	2c	33.6	2.24	52.8
	Fe_2(8f/1:12)	4e	19.9	1.33	
	Nitride	4e	27.2	1.6	
	Fe_{11} (mixed)	8j	20.6	1.37	
	Nitride	8j	30.4	1.92	
	Fe_4(8j/1:12)	4i	20.5	1.37	
	Nitride	4i	32.1	1.88	
	Fe_8(18f/2:17)	8j	19.1	1.28	
	Nitride	8j	25.7	1.72	
	Fe_9 (mixed)	8j	19.8	1.32	
	Nitride	8j	27.9	1.80	
	Fe_5(18h/2:17)	4i	17.8	1.19	
	Nitride	4i	29.3	1.95	
	Fe_{10}(18h/2:17)	8j	17.8	1.19	
	Nitride	8j	29.3	1.95	
	Fe_3(8*i*/1:12)	4g	28.9	1.93	
	Nitride	4g	34.4	2.02	
	Fe_6 (mixed)	4i	25.6	1.70	
	Nitride	4i	33.4	2.1	
	Fe_7 (mixed)	4i	25.6	1.70	
	Nitride	4i	33.4	2.1	

[a] Data from [30]; the B_{hf} values are averages from the original data.
[b] Data from [36].

Usually these sites are considered with ten TM and two R nns, forming (0, 0, 12, 0) polyhedra, as in the 1:12 8f site (figure 5(a)). Figure 8 shows the arrangement of nns around the group-B sites, the 18f site in 2:17R and the 1:12 8j site that shares a similar (0, 0, 12, 0) environment [34] with group-B sites as well. This figure shows that Fe_4 has ten TM nns whereas the 11th TM nn,

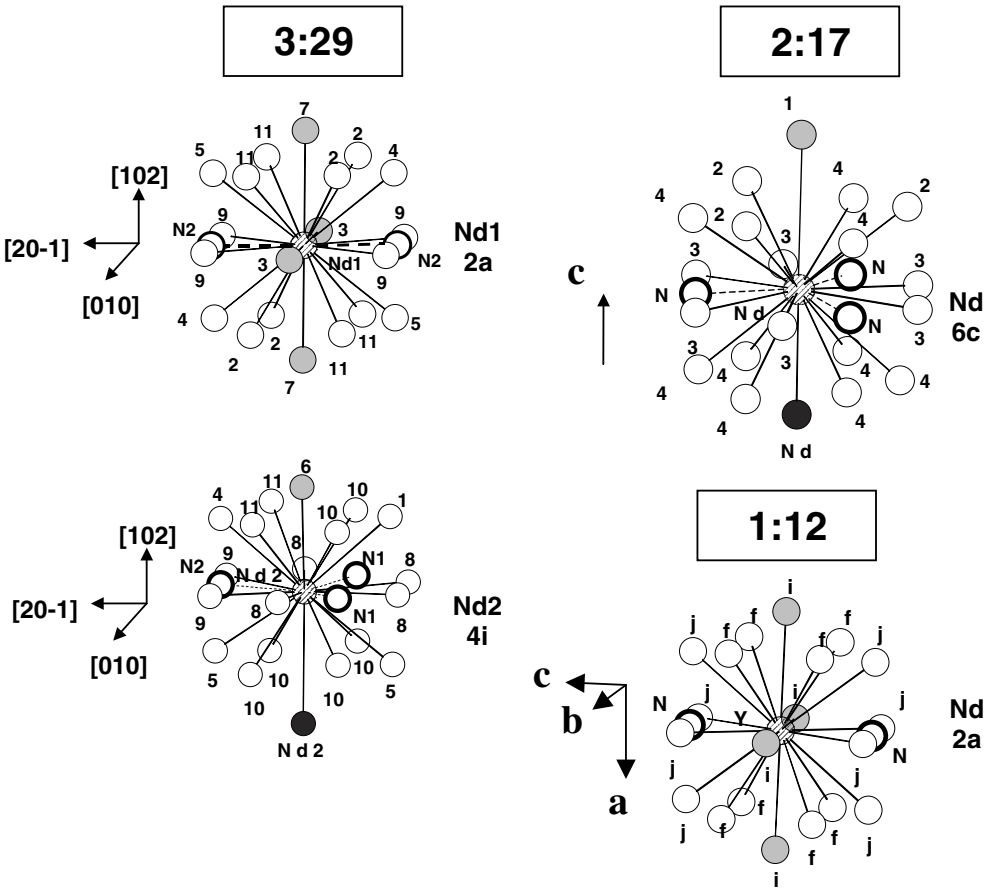

Figure 5. Arrangement of nns around the Nd_1 and Nd_2 sites in 3:29, the Nd 6c site in 2:17R and around the Nd 2a site in the 1:12 structure. For clarity, only the numbering of TM nns is shown. Grey circles indicate statistically occupied (Fe, Ti) sites, hatched circles indicate R sites and bold circles indicate nitrogen sites. The tris-orthogonal crystallographic directions define the orientation of the cluster in the corresponding lattice.

Fe_5, resides further away, at a distance of 3.896(8) Å from the central atom, without modifying the WS polyhedron (figure 5(a)). The other two sites, Fe_8 and Fe_9, have the symmetrically equivalent atoms Fe_8 and Fe_9 (figure 6) at a distance of 3.584(5) and 3.709(3) Å respectively. These atoms can be viewed as the 11th TM nns since at these distances the WS cell becomes a (0, 1, 10, 2) polyhedron (figure 5(a)). The same environment is observed in the case of the 18f site in 2:17R and the 8f site in 1:12 structures. Upon nitrogen uptake one nitrogen occupies a site in between the distance of Fe_4–Fe_5, Fe_8–Fe_8 and Fe_9–Fe_9, creating a fourfold facet with much larger area, thus transforming the three sites into 13-fold environments with (0, 1, 10, 2) polyhedra (figure 5(c)), as the 18f site [35] in 2:17R and the 8f site in 1:12. Since the inclusion or not of these extra nns does not alter the volumes of the corresponding WS cells (table 2) in the 3:29, and the relative [14] Nd_2Fe_{17} or $Nd_2Fe_{16.3}Ti_{0.7}$ compounds (see table 3), this 13-fold cell was overlooked for the discussion of their magnetic properties in past studies [9]. However, as is clearly seen in figure 5 for the case of nitrogen uptake, such a (0, 0, 12, 0) → (0, 1, 10, 2) transformation in Fe cells is expected to affect the magnitude of the site magnetic moment because it changes the shape of the Brillouin zone as well.

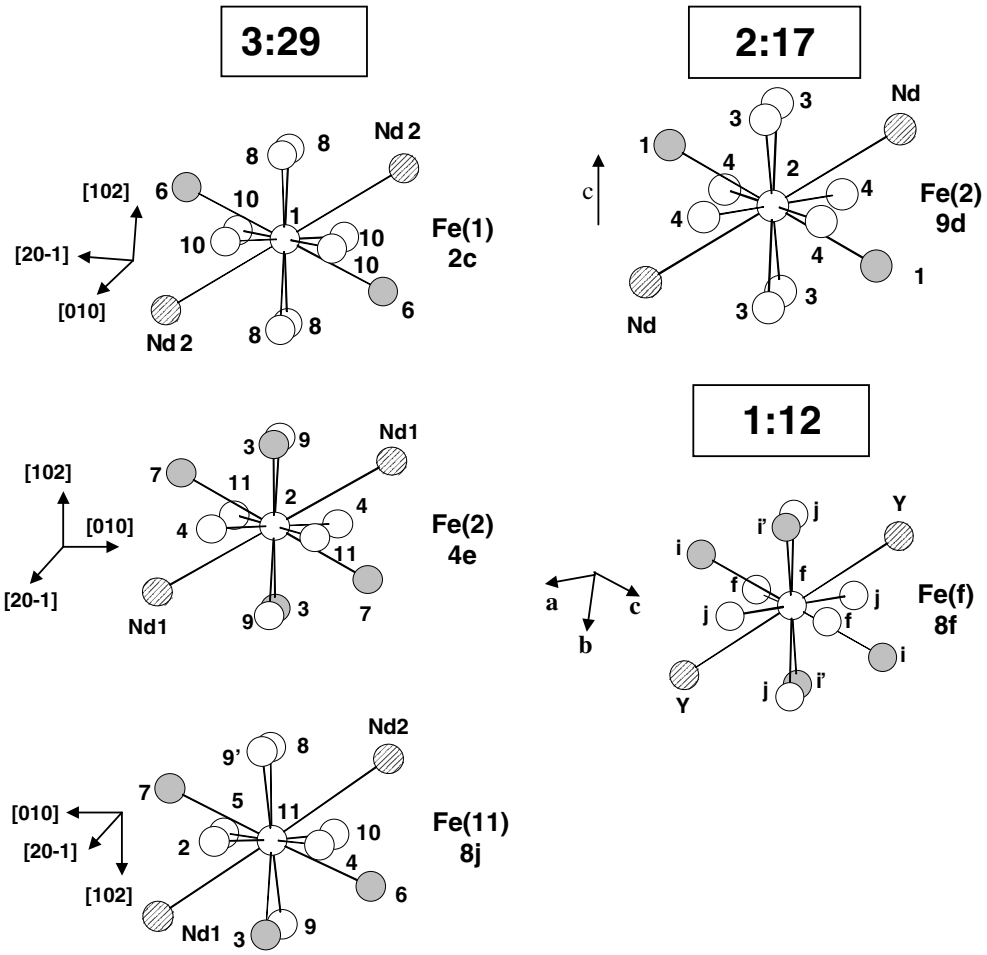

Figure 6. Arrangement of nns around the group-A sites in 3:29, the Fe_2 (9d) site in 2:17R and around the 8f site in the 1:12 structure. For clarity, only the numbering of TM nns is shown. Grey circles indicate statistically occupied (Fe, Ti) sites, and hatched circles indicate R sites. The tris-orthogonal crystallographic directions define the orientation of the cluster in the corresponding lattice.

Group C includes Fe_5-4i [Fe(9)] and Fe_{10}-8j [Fe(10)] atoms, corresponding to the 2:17R 18h site. These atoms have only nine TM nns and exhibit the lowest moments in 3:29 and 2:17R structures [30, 33]. Comparison of WS cell volumes (tables 2 and 3) shows similar values as well. In addition, their 12-fold environments transform to 13-fold environments upon nitrogen uptake, following the Frank–Kasper sequence $(0, 0, 12, 0) \rightarrow (0, 1, 10, 2)$, as the 18h site does [35] in the 2:17R structure. Figure 9 shows the atomic arrangement of nns around the group-C sites, and the 18h site in the 2:17R structure. The special feature of group-C and 2:17R 18h sites is that all exhibit three Nd ions as nns. Such an environment does not exist in the $ThMn_{12}$ type of structure.

Group D includes Fe_3-4i [Fe(6)], Fe_6-4i [Fe(3)] and Fe_7-4g [Fe(2)] atoms, corresponding to the 6c site (dumbbell site). These 14-fold sites (figure 8) form typical 14-fold Frank–Kasper polyhedra, and thus are involved in $-72°$ disclinations along the R–(TM–TM) bond lines with two sixfold facets in opposite directions (vertical to the R–TM–TM bond line). They have

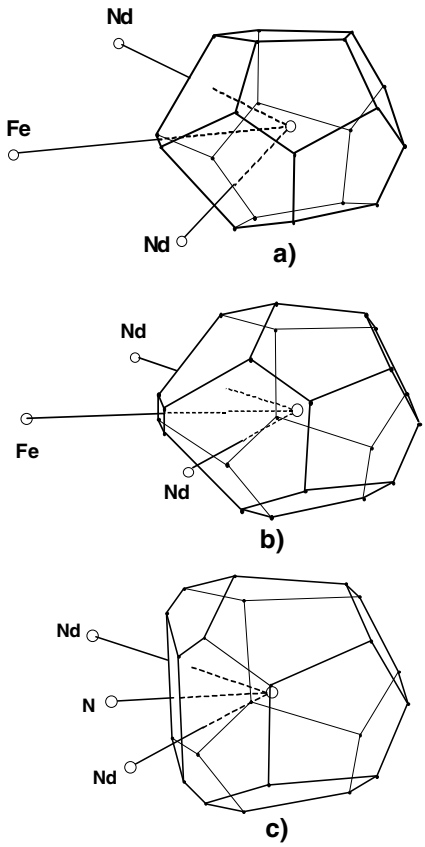

Figure 7. The three cases for the generation of a 13-fold (0, 1, 10, 2) polyhedron from the (0, 0, 12, 0) WS cell are shown. (a) The 13th TM nn is far away from the central atom and the bond line toward this neighbour intersects an edge of the polyhedron. The WS cell remains (0, 0, 12, 0). (b) The 13th TM nn is closer to the central atom and a fourfold facet is generated together with two hexagonal facets. This is the case of Fe_8 and Fe_9 sites in 3:29 before nitrogen uptake. (c) Formation of the (0, 1, 10, 2) WS cell after the insertion of nitrogen in group-B, C 3:29 sites or 2:17R 18f sites or 1:12 8j sites.

13 TM nns, one Nd nn, exhibit the largest moments [30, 33] in 3:29 and 2:17R structures and are preferentially occupied by the stabilizing element Ti. Table 1 displays Fe occupancies of 84% for Fe_3 [Fe(6)], 70% for Fe_6 [Fe(3)] and 76% for Fe_7 [Fe(2)], which are in agreement with previous results [17]. In comparison, 34% of Ti atoms occupy [30] the dumbbell 6c site in $Nd_2Fe_{16}Ti$, indicating a close connection between the 14-fold WS cell and the preferential substitution of the stabilizing element in these structures. Comparison of WS cell volumes (tables 2 and 3) shows similar values as well, which are the largest among the others. In addition, their 14-fold environments (0, 0, 12, 2) remain intact upon nitrogen uptake (tables 2 and 3), indicating a relative isolation from nitrogen sites. Figure 10 shows the atomic arrangement of nns around the group-D sites, the dumbbell 6c site in 2:17R and the 1:12 8i site. This figure reveals that the 1:12 8i site shares a similar (0, 0, 12, 2) environment [34] and is preferentially occupied by the stabilizing element [36] Ti in the same way as the corresponding 3:29 sites. Major disclination lines are defined along the Nd_1–Fe_3–Fe_3, Nd_2–Fe_6–Fe_7 and Nd_1–Fe_7–Fe_6 directions which correspond [26] to hard-magnetic directions [010] ∥ (a-axis of 1:12) and [102] ∥ (c-axis of 2:17) in 3:29, respectively.

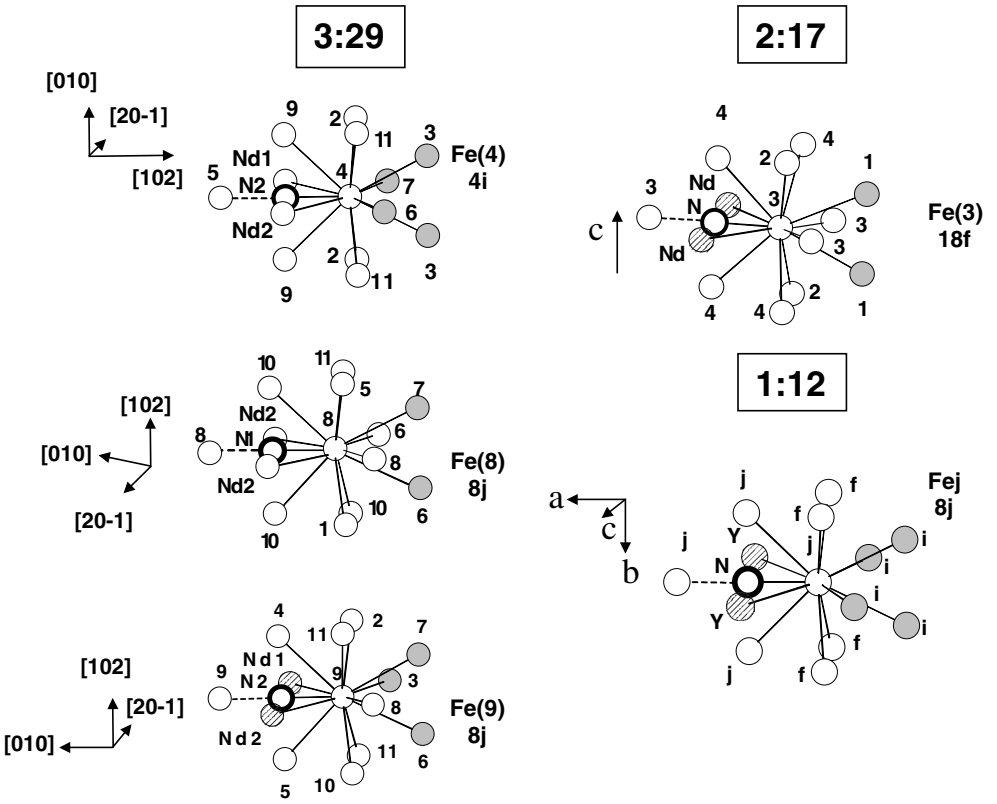

Figure 8. Arrangement of nns around the group-B sites in 3:29, the Fe_3 (18f) site in 2:17R and around the 8j site in the 1:12 structure. For clarity, only the numbering of TM nns is shown. Grey circles indicate statistically occupied (Fe, Ti) sites, hatched circles indicate R sites and bold circles indicate N sites. The tris-orthogonal crystallographic directions define the orientation of the cluster in the corresponding lattice.

Note that the average atomic distances $\langle r_i \rangle$ in the four groups (i = A, B, C, D) of the 3:29 structure are closer to the values of the corresponding nn distances in $Nd_2(Fe, Ti)_{17}$ instead of those in Nd_2Fe_{17} (tables 2 and 3). In addition, the corresponding $NdFe_{11}Ti$ sites exhibit $\langle r_i \rangle$ values [36] of $\langle r(8f) \rangle \approx 2.52$ Å, $\langle r(8j) \rangle \approx 2.59$ Å and $\langle r(8i) \rangle \approx 2.71$ Å, which are relevant to the values of groups A, B and D respectively. Furthermore, tables 2 and 3 reveal that the WS volumes (WSVs) follow the same sequence: WSV(A) < WSV(B) < WSV(C) < WSV(D) for the four groups in 3:29 and for the corresponding sites of the 2:17R phases, where WSV(9d) < WSV(18f) < WSV(18h) < WSV(6c). This trend holds and for the corresponding 1:12 sites as long as the stabilizing element (Ti in our case) occupies preferentially only the 8i site (which is similar to group-D environment). However, a reversal occurs in the order of the WSV(A) and WSV(B) sizes upon nitrogen uptake. Specifically, the sequence of WSVs becomes (tables 2 and 3) WSV(B) < WSV(A) < WSV(C) < WSV(D) in 3:29, WSV(18f) < WSV(9d) < WSV(18h) < WSV(6c) in 2:17R and WSV(8j) < WSV(8f) < WSV(8i) in 1:12 nitrides [36]. This shrinkage of the 3:29 WSV(B), 2:17R WSV(18f) and WSV(8j) is clearly *due to the 13th nitrogen nn in these sites* whereas the sites of group-A, 2:17R 9d and 1:12 8f do not have nitrogen nns to truncate their WS polyhedra. It is worth noting that although group-C and 2:17R 18h environments transform into (0, 1, 10, 2) polyhedra upon nitrogen uptake the

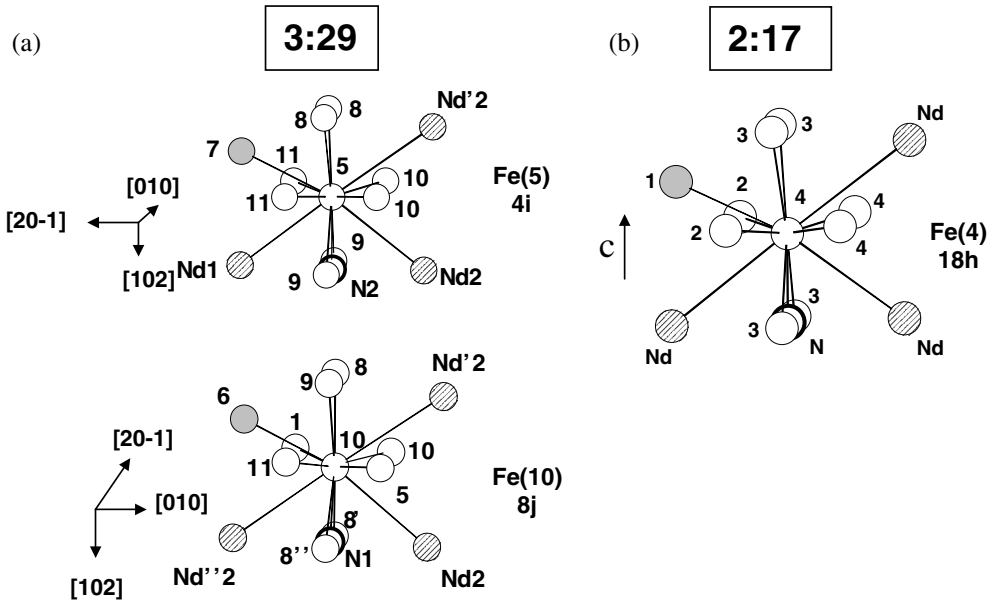

Figure 9. Arrangement of nns around the group-C sites in 3:29, and the Fe_4 (18h) site in the 2:17R structure. For clarity, only the numbering of TM nns is shown. Grey circles indicate statistically occupied (Fe, Ti) sites, hatched circles indicate R sites and bold circles indicate nitrogen sites. The tris-orthogonal crystallographic directions define the orientation of the cluster in the corresponding lattice.

induced strain, and thus the maximum observed WSV shrinkage, is accommodated in the vicinal group-B (2:17R 18f) environments that are beneath the fourfold Nd_1–Fe_9–Nd_2–Fe_9 and Nd_2–Fe_8–Nd_2–Fe_8 (2:17R, Nd–Fe_3–Nd–Fe_3) facets in figure 9.

All the results in this section reveal a global character of WS volume relations in RFe-rich structures that emerge from the parent 1:5 ($CaCu_5$ type of structure) phase [26]. Such volume relations indicate that an interplay of volume and d-band fillings is essential for the formation of identical (Frank–Kasper-like) environments. Since magnetism in Fe-rich compounds is determined mainly by the dependence of the electronic levels on local structure (spin-fluctuation theory [37]), rather than the Bloch nature of the wavefunctions, there are four important aspects of short-range order for 3d magnetism. These are the coordination number Z_{TM}, type, distance and symmetry of the nns about a given TM site. The contents of this section show that all the information about these four aspects is hidden in the WS cell polyhedron for a given type of nn. In the next section we will try to unveil the hidden information from the calculated WS cell polyhedra in order to relate it to both the magnitude and the anisotropy of site magnetic moments in the examined category of RFe-rich compounds.

5. Disclination nets and basic magnetism

In this section the long-standing problem that concerns relationships between local environments and the relative strength of the different magnetic moments on the different Fe sites [38] is revisited. Our motivation is based

(i) on the experimental finding [39] that the saturation magnetizations of $Nd_3Fe_{29-x}Ti_x$ compounds ($1.6 \leqslant x \leqslant 1.2$) can be estimated from a combination of the saturation magnetizations of the 2:17R and 1:12 units in a ratio of 1:1, and

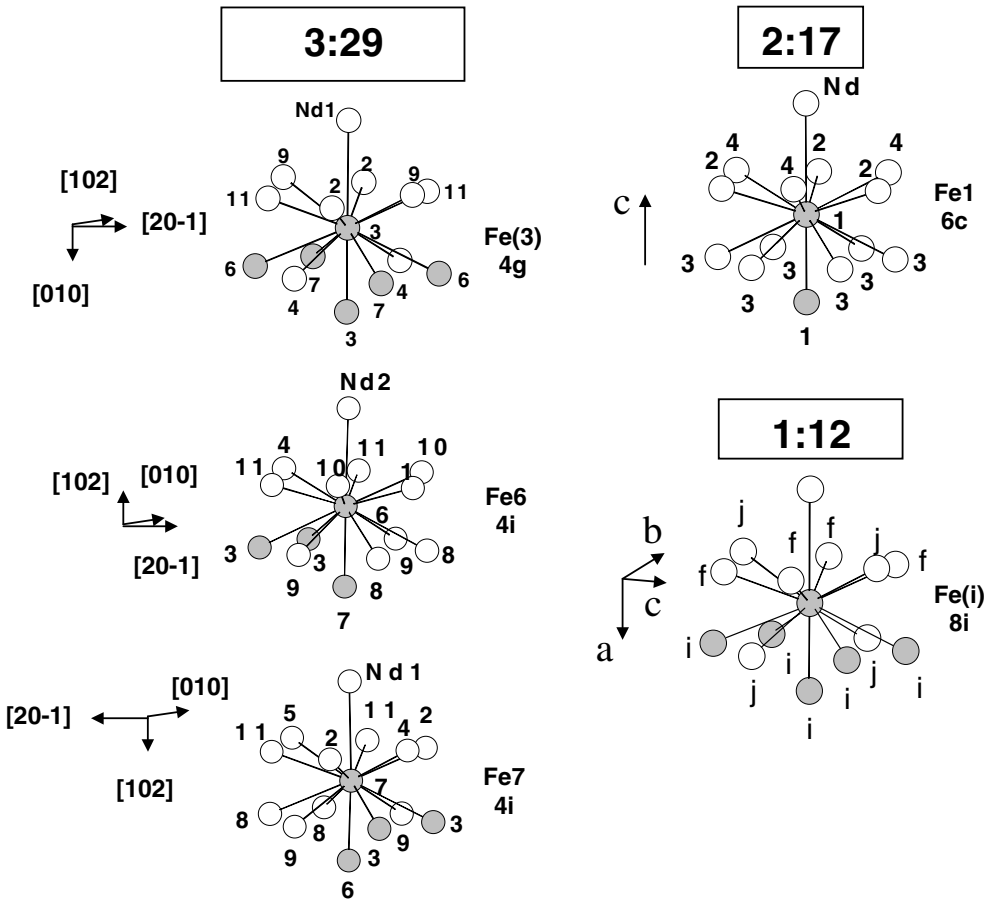

Figure 10. Arrangement of nns around the group-D sites in 3:29, the Fe_1 (6c) site in 2:17R and around the 8ji site in the 1:12 structure. For clarity, only the numbering of TM nns is shown. Grey circles indicate statistically occupied (Fe, Ti) sites and hatched circles indicate R sites. The tris-orthogonal crystallographic directions define the orientation of the cluster in the corresponding lattice.

(ii) on the realization that both the occurrence of disclination lines and the relatively larger WS cell volumes in 14-fold environments lead to larger μ^i_{Fe} values [13, 38].

In accordance, the above-described results show that the large-volume, large-moment sites in $Nd_3(Fe, Ti)_{29}$, like the largest sites in Nd_2Fe_{17}, $Nd_2Fe_{16.3}Ti_{0.7}$, $NdFe_{11}Ti$ and $Nd_2Fe_{14}B$ compounds, are the 14-fold coordinated $(0, 0, 12, 2)$ Frank–Kasper (group-D) environments. All the other sites are 12- or 13-fold coordinated. As suggested by Watson *et al* [14], the existence of six TM nns in one direction instead of five leads to a location of these nns at larger interatomic distances from the central atom, thus increasing the WS volume of this site. Thus, usually, the largest moments are associated with the sixfold facets in the 14-fold environment.

Figure 10 shows that the 3:29 structure accommodates three such environments whereas for the 2:17R and 1:12 structures there is only one 14-fold environment in each one. The estimated dumbbell (TM–TM) distances are the shortest (about 2.45 Å) in group D, with bonds crossing a sixfold facet along either direction, having six TM nns that lie further out

radially from the bond line. Remarkably, all the statistically occupied (Fe, Ti) sites reside between the dumbbell (Fe_3–Fe_3), -(Fe_6–Fe_7) pairs whereas the sites between the Nd–Fe_3, Nd–Fe_6, Nd–Fe_7 bonds are occupied only by Fe atoms. This configuration increases the *chirality* (clusters are said to be *chiral* when they are not superimposable on their mirror images) along the Nd–(TM–TM) disclinations, resembling the configuration of the corresponding 8i 1:12 site while it is different from that in the 6c 2:17R site. Since different (Fe, Ti) occupancies cause variations in the strength of exchange coupling among the three group-D environments, it is expected that the smaller number of statistically occupied (grey) (Fe_6, Ti) and (Fe_7, Ti) sites (which are three relative to five around the Fe_3 environment) around the Fe_6 and Fe_7 environments (figure 8) should give the highest moments at Fe_7 and Fe_6 sites. This conclusion is in accordance with hyperfine fields (B_{hf}) obtained [30] for the $Nd_2Fe_{16.3}Ti_{0.7}$ compound, where the corresponding dumbbell 6c site exhibits two different B^i_{hf} values (i = 6c or 6c′) that differ by about 6 T ($\sim$0.4 μ_B) due to one Ti nn (figure 8). In addition, it is in qualitative agreement with calculated [40] local moments for the Fe_6 and Fe_7 sites in $Nd_3Fe_{28}Ti$, but it shows that the calculated moment of Fe_3 (which is 1 μ_B less than the Fe_6 and Fe_7 moments) is unacceptably low for one of the three group-D (14-fold) environments.

TM atoms at dumbbell sites is the peculiar characteristic of 1:12, 2:17R and 3:29 structures. Each of them can be derived from the RTM_5 structure by replacing a fraction of R atoms with TM dumbbells: $R_{1-\delta}(2TM)_\delta TM_5$, where $\delta = 1/3, 1/2$ or $2/5$ corresponds to 2:17, 1:12 or 3:29 respectively. In many cases in the past this characteristic has been considered as the main source for the relatively low T_c values (compared with α-Fe): $T_c \sim 2J(r)Z_{TM}S(S+1)/3k_B$, since short Fe–Fe distances stabilize bonding states between two atoms that favour paired-antiparallel spins, thus weakening the distance-dependent interatomic exchange integral $J(r)$ (Bethe–Slater curve). However, recent studies [41] on $Sm_2(Fe)_{17}X$ (X = C or N) have shown that the dumbbell (TM–TM) distances remain almost the same in the nitride and the host Sm_2Fe_{17} structure whereas there is a substantial increase of T_c (=388 $\rightarrow$ 750 K) upon N uptake. In accordance, the estimated dumbbell (Fe_3–Fe_3),-(Fe_6–Fe_7) interatomic distances (figure 8) are between 2.44 and 2.5 Å, are the shortest in group D, are comparable with bond lengths in the fivefold facets of groups A, B and C and do not change much in the nitride. In view of these results, the role of interstitially substituting elements around the dumbbell sites should be re-considered.

Figures 8 and 9 indicate that N atoms occupy coplanar sites around the Nd site without changing the (TM–TM) distances around the dumbbell sites (figure 10). It becomes more evident from the areas of the hexagonal facets in the dumbbell sites (about 3.1 Å^2) which remain the same before and after nitrogen uptake. In addition, the 20-fold Nd environments (0, 0, 12, 8) transform to non-Frank–Kasper cells upon nitrogen uptake in $Nd_3(Fe, Ti)_{29}$, forming a larger number of six-edged and four-edged facets. Figure 5 shows the atomic arrangement of nns around the two inequivalent R sites (2a and 4i) in 3:29, the 6c R site in 2:17R, that shares the same environment as the 3:29 4i site, and the 2a R site in 1:12, that shares the same environment as the 3:29 2a site. The calculated areas of the facets show that these extra sixfold facets, which are created either at 12-fold (group-B and C sites) or 20-fold (R sites) environments upon nitrogen uptake, exhibit smaller areas than the fivefold facets because their disclination lines do not couple TM–TM, R–R or R–TM atoms as the sixfold facets do in 14-fold environments. In addition, the (0, 0, 12, 2) cell has two sixfold bond lines lying in a straight (disclination) line whereas the (0, 1, 10, 2) cell (figure 5(c)) has the two sixfold bond lines 120° away from each other, defining two disclination lines in a plane. Thus, *the nitrogen-induced sixfold facets are distinct from the sixfold facets in 14-fold environments and should influence in a different way the site magnetic moments and the anisotropy of the nitrides*.

Figures 6–10 show that a number of 3:29 environments exhibit exactly the same site symmetry and Ti or N occupancies as the corresponding 2:17R, 1:12 environments, whereas some other 3:29 environments exhibit intermediate Ti occupancies between the $Nd_2Fe_{16.3}Ti_{0.7}$ and $NdFe_{11}Ti$ site occupancies. Assuming a mutual relationship in site magnetic moments and anisotropies among the site environments of 3:29, 2:17R and 1:12-type compounds, a comparative analysis of the site hyperfine fields $B^i_{\rm hf}$ among the three kinds of compound can be carried out. In analogy with [39], we consider that $Nd_3Fe_{27.3}Ti_{1.7} \equiv Nd_2Fe_{16.3}Ti_{0.7} + NdFe_{11}Ti$. To the best of our knowledge, there are no available site magnetic moments for 3:29 compounds from *spin-polarized* NPD experiments (which is the only reliable NPD technique to extract experimental moments from ferromagnetic powders with low-symmetry crystal structures) or high-quality single crystals. For this reason our analysis is based only on ^{57}Fe Mössbauer data, which provide the best local probe of Fe moments from the 11 iron sites in the 3:29 structure. Thus, we assign $B^i_{\rm hf}$ values for the 3:29 type of compound from the available experimental values obtained at room temperature for [30] $Nd_2Fe_{16.3}Ti_{0.7}$ and [36] $NdFe_{11}Ti$.

The visible resemblance in site symmetry between the 3:29 and 2:17R, 1:12 environments (figures 6, 8–10) allows a tentative assignment of site $B^i_{\rm hf}$ values in table 4 for the $Nd_3Fe_{27.3}Ti_{1.7}$ and its nitride from the known values [30, 36] of the constituent 2:17R and 1:12 blocks. To a good first approximation $B^i_{\rm hf} = A_{\rm hf}\mu^i_{\rm Fe}$, where the constant of proportionality $A_{\rm hf}$ depends on details of the magnetization density at the site and the environment in which the site finds itself. The choice of $A_{\rm hf}$ is a real issue in determining the $\mu^i_{\rm Fe}$ values for the examined compounds. A coefficient of 15 T/$\mu_{\rm B}$ has been obtained from experiments on Y–Fe systems [36]. However, for $YTiFe_{11}N_x$ an $A_{\rm hf} = 17.4$ T/$\mu_{\rm B}$ was found [36] to be more appropriate. We have used these coefficients to estimate $\mu^i_{\rm Fe}$ values from which we have estimated the saturation magnetization $M_{\rm s}$(Fe) of *iron sublattices* per formula unit (fu) to compare with known [30, 36, 39] experimental values. It is worth noting that the used $B^i_{\rm hf}$ values were determined from ^{57}Fe Mössbauer spectra and for this reason the hyperfine field contributions from Nd site moments are not included in table 4, but they should be taken into account for the estimation of $M_{\rm s}$ to compare with bulk magnetization measurements. Note also that the comparatively low $M_{\rm s}$(Fe) obtained for $Nd_2Fe_{16.3}Ti_{0.7}$ at room temperature is due to its low $T_{\rm c}$(∼380 K).

An $M_{\rm s}$(Fe) $= 27.3(\sum \mu^i_{\rm Fe})/11 = 42.6\ \mu_{\rm B}$/fu was derived for $Nd_3Fe_{27.3}Ti_{1.7}$, which is in good agreement with an $M_{\rm s} = 44.8\ \mu_{\rm B}$/fu, obtained from isothermal magnetization measurements [39], if an average value of 2.2 $\mu_{\rm B}$ is added to take into account the contribution of Nd ion moments at room temperature from the two Nd sites (an $\mu_{\rm Nd} = 1.3(2)\ \mu_{\rm B}$ was estimated for the 2:17R 6c Nd site from NPD data [30] at 295 K). In comparison to a $\langle B_{\rm hf}\rangle = 21.1$ T for [43] $Nd_3(Fe, Ti)_{29}$ at room temperature, the estimated $\langle B_{\rm hf}\rangle = 21.2$ T from table 4 matches perfectly. This result indicates that the selected site magnetic moments can be reliable estimates of actual $\mu^i_{\rm Fe}$ values in $Nd_3Fe_{27.3}Ti_{1.7}$. Thus, the assignment of $B^i_{\rm hf}$ values for the group-D sites in table 4 shows that the calculated [40] local moment for Fe_3 is unacceptably low in $Nd_3Fe_{28}Ti$. Applying the same practice for $Nd_3Fe_{27.3}Ti_{1.7}N_x$ an $M_{\rm s}$(Fe–N) $= 52.8\ \mu_{\rm B}$/fu was derived when an $A_{\rm hf} = 17$ T/$\mu_{\rm B}$ was used [36] for the 1:12 type of nitrided site whereas for the rest an $A_{\rm hf} = 15$ T/$\mu_{\rm B}$ was applied. In comparison to a $\langle B_{\rm hf}\rangle = 31.0$ T(∼2.06 $\mu_{\rm B}$/Fe), obtained [42] at room temperature for a nominal $Nd_3(Fe, Ti)_{29}N_{4.5}$ composition, and to a $\langle B_{\rm hf}\rangle = 29.4$ T for [43] $Nd_3(Fe, Ti)_{29}N_4$, the estimated $\langle B_{\rm hf}\rangle = 30.6$ T(∼2.04 $\mu_{\rm B}$/Fe) from table 4 matches perfectly.

In addition, our analysis can provide a simple interpretation of the easy-magnetization direction (EMD) observed [26] in 3:29 compounds with R = Y or Gd (iron sublattice anisotropy) by relating these EMDs to disclination lines that occur in 1:12 and 2:17R

compounds. Disclination nets for the 1:12, 2:17 and 3:29 phases are shown in figures 11 and 12. Every disclination net is formed with bond lines connecting atoms across sixfold facets. Disclinations connecting two subsequent R–R ions or alternating repetitions of (rare-earth)–(dumbbell) sites, –R–(TM–TM)–, are called principal. The 2:17R structure exhibits principal disclination lines that connect [–R–R–(TM–TM)–] repetitions of atoms along the *c*-axis (solid lines in figure 9(b)). Normal to this direction there are disclinations of [–R–TM–] type, called secondary, that lie in the *a*–*b*-plane (solid lines in figure 9(b)) through the sixfold facets of the 18f site polyhedron. In R_2Fe_{17} (R = Nd, Gd) the EMD is within [26] the *a*–*b* 2:17R plane as well. Out-of-plane [–R–TM–] secondary disclinations are created (dashed lines in figures 11(b) and 12(b)) through the sixfold facets of the 18h site polyhedron, forming a two-dimensional net upon nitrogen uptake. In the 1:12 structure the principal disclinations form a tetragonal, two-dimensional net within the (001) plane and their lines are of the [–R–(TM–TM)–] type. Before nitrogen uptake there are no secondary disclinations (figure 9(a)) because there are no sixfold facets in the polyhedron of the 8j site. However, the [–R–TM–] type of line appears upon nitrogen uptake (dashed lines in figures 11(a) and 12(a)) that form zig-zag lines along the [001] direction. In $RFe_{11}Ti$ (R = Y, Nd, Gd) compounds the EMD is along the *c*-axis (‖[001]) at room temperature [44].

In the 3:29 structure the principal disclination lines lie in the $(20\bar{1})$ plane and they are of [–R–R–(TM–TM)-R–(TM–TM)–] type (a mixed sequence of 1:12 and 2:17R types) along the [102] ‖ (*b*-axis of 1:12) ‖ (*c*-axis of 2:17R) direction and of [–R–(TM–TM)–] type (1:12-like) along the [010] ‖ (*a*-axis of 1:12) direction within this plane (figures 11(c) and 12(c)). Within the (102) plane there are secondary disclination lines of [–R–TM–] type, passing through the sixfold facets of Fe_8 and Fe_9 environments (solid lines in figures 11(c) and 12(c)). Additional, out-of-plane [–R–TM–] disclinations are created upon nitrogen uptake (dashed lines in figures 11(c) and 12(c)) due to formation of sixfold facets in Fe_5 and Fe_{10} sites. All the secondary disclinations form a two-dimensional net, as in the 2:17R structure (figures 11(b) and 12(b)), that is within the (102) plane. It is worth noting that all the secondary disclinations form octahedra, enclosing a nitrogen interstitial atom at the centre of each octahedron. Each octahedron in figures 9 and 10 indicates a nitrogen interstitial, revealing their distribution within the 1:12, 2:17R and 3:29 lattices. Figure 12(c) shows that along the *b*-axis run principal disclinations of [–R–(TM–TM)–] type whereas along the $[20\bar{1}]$ EMD [26, 45] run only secondary disclinations of [–R–TM–] type.

Thus, as a rule of thumb, the EMD of the *iron sublattice* is always along the [–R–TM–] type of secondary disclination and normal to principal disclination lines that define hard-axis directions in the three types of structure. However, in the case of Co-rich [1] 1:12, 2:17 and [46, 47] 3:29 structures, usually, the EMD of the Co sublattice is observed to be orthogonal to that of the Fe sublattice, and thus is along the principal disclination lines. Besides the existing difference in the electronic density of states at the Fermi level between Fe and Co-rich RTPMs, in our structural model, this alternation of EMD can be attributed to the difference between Fe and Co atomic radii, that alters the interatomic distances in the WS polyhedra. This last argument remains to be shown quantitatively in a future study.

6. Summary and conclusions

In summary, it is shown that Frank–Kasper-like structures provide an adequate method for the definition of M_s, μ^i_{Fe} and EMD in the examined class of RFe-rich compounds. Specifically, we have the following.

(i) The crystal structures of $Nd_3Fe_{27.60(3)}Ti_{1.40(3)}$ and $Nd_3Fe_{27.78(5)}Ti_{1.22(5)}N_{3.80(6)}$ intermetallics have been determined from Rietveld refinement of high-resolution NPD data

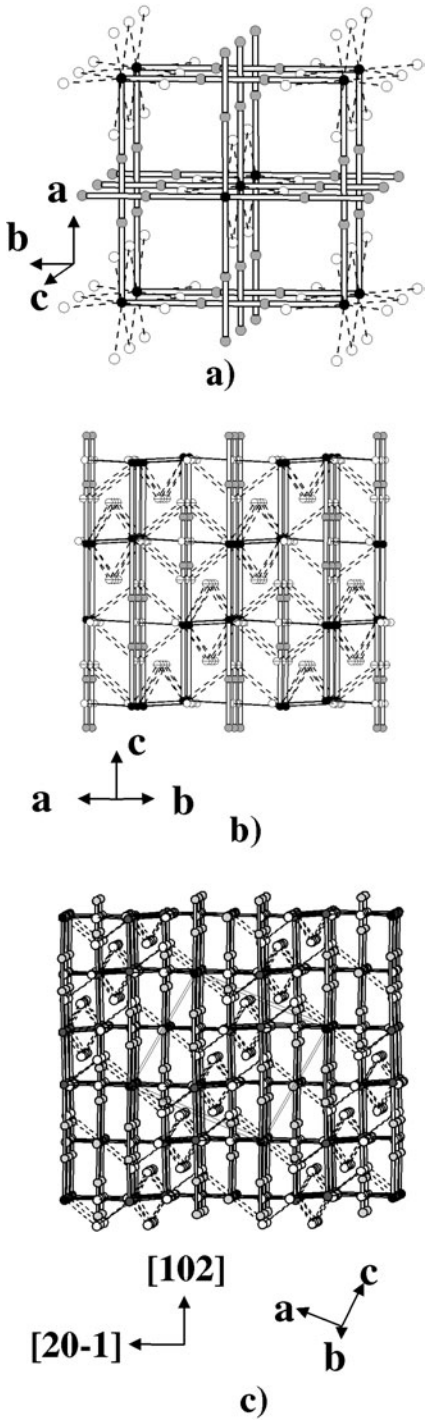

Figure 11. Three-dimensional disclination nets for (a) the 1:12 structure; (b) the 2:17R structure and (c) the 3:29 structure, where the unit cell is shown as well. Solid lines are principal disclinations and dashed lines are the secondary disclinations that are created after nitrogen uptake. Dark circles denote Nd atoms, grey circles denote dumbbell TM atoms and open circles denote group-B or C TM atoms or the corresponding site TM atoms in 1:12 and 2:17R structures.

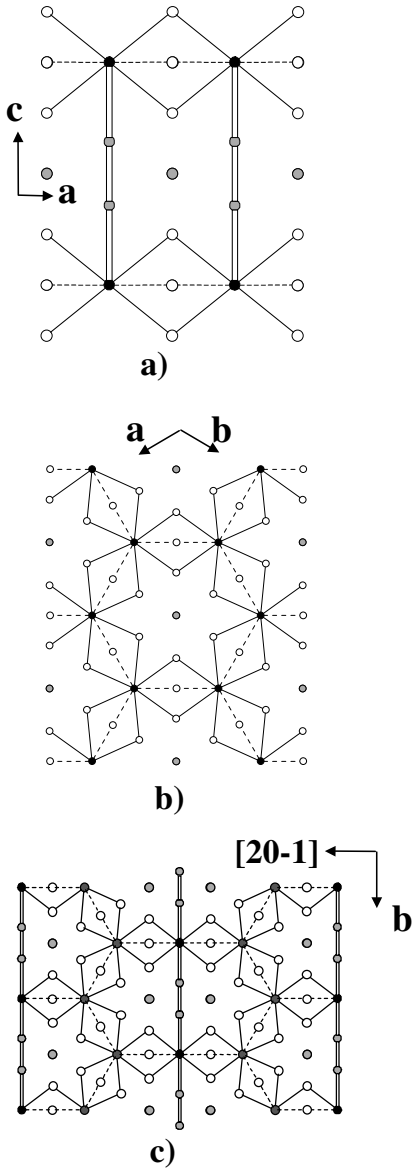

Figure 12. Two-dimensional disclination nets within (a) the 1:12 a–c plane; (b) the 2:17R a–b plane and (c) the monoclinic 3:29 (102) plane. Double-solid and single-solid lines are principal and secondary disclinations respectively within the plane of the paper whereas dashed lines are the zig-zag, in-and-out of the paper plane, secondary disclinations that are created after nitrogen uptake. Dark circles denote Nd atoms, grey circles denote dumbbell TM atoms and open circles denote group-B or C TM atoms or the corresponding site TM atoms in 1:12 and 2:17R structures.

at room temperature. These high-precision crystal structure parameters were used for the calculation of the corresponding WS cells. The construction of the WS polyhedra has revealed that some 12-fold (group-A) environments and the 14-fold (group-D, dumbbell) environments remain intact upon nitrogen uptake whereas some other 12-fold

(group-B, C) environments transform according to the Frank–Kasper sequence [0, 0, 12, 0] → [0, 1, 10, 2].

(ii) The WS cells were calculated for the 12-, 13-and 14-fold Frank–Kasper-like polyhedra of 1:12 and 2:17R types of structure. A global character of WS volume relations has been revealed, where the corresponding WSVs follow the same sequence for the three types of structure: WSV(A) < WSV(B) < WSV(C) < WSV(D) in $Nd_3(Fe, Ti)_{29}$, WSV(9d) < WSV(18f) < WSV(18h) < WSV(6c) in $Nd_2Fe_{16.3}Ti_{0.7}$ and WSV(8f) < WSV(8j) < WSV(8i) in $NdFe_{11}Ti$. However, a reversal occurs in the order of 3:29 WSV(A), 2:17R WSV(9d), 1:12 WSV(8f) and 3:29 WSV(B), 2:17R WSV(18f), 1:12 WSV(8j) sizes upon nitrogen uptake, revealing that the induced strain, and thus the maximum observed WSV shrinkage, is accommodated mainly in the vicinal group-B (2:17R 18f, 1:12 8j) environment.

(iii) Disclination nets have been constructed for the three types of structure and a rule of thumb is revealed for the EMD. It was shown that the EMD of the iron sublattice is always along the [–R–TM–] type of secondary disclination line and it is perpendicular to the principal disclinations which define the hard axes.

(iv) A systematic analysis of the site hyperfine fields B_{hf}^{i} in the three kinds of compound led to a successful estimation of M_{s} (close to experimental M_{s}) from a tentative assignment of site magnetic moments in $Nd_3Fe_{27.3}Ti_{1.7}(\equiv Nd_2Fe_{16.3}Ti_{0.7} + NdFe_{11}Ti)$.

Acknowledgments

The experiment at the ISIS neutron spallation source was supported by the European Union through its Training and Mobility of Researchers Programme for Large Scale Facilities. We thank Dr R M Ibberson for his help during the neutron diffraction experiment and Dr M Gjoka for sample preparation.

References

[1] Buschow K H J 1997 *Handbook of Magnetic Materials* vol 10 (Amsterdam: Elsevier) chapter 4
[2] Coey J M D and Sun H 1990 *J. Magn. Magn. Mater.* **87** 251
Otani Y, Hurley D F P, Sun H and Coey J M D 1991 *J. Appl. Phys.* **69** 5584
[3] Muller K H, Cao L, Dempsey N M and Wendhausen P A P 1996 *J. Appl. Phys.* **79** 5045
[4] Yang F, Nasunjilegal B, Wang J, Zhu J, Qin W, Tang N, Zhao R, Hu B-P, Wang Y-Z and Li H-S 1995 *J. Phys.: Condens. Matter* **7** 1679
Guoa H Q, Nasunjilegala B, Yanga F-M, Tanga N, Qina W D, Wanga J L, Zhua J J, Hu B-P, Wang Y Z and Li H-S 1995 *J. Alloys Compounds* **222** 27
[5] Marasinghe G K, Ezekwenna P C, James W J, Hu Z and Yellon W B 1997 *J. Appl. Phys.* **81** 5103
[6] Koyama K and Fujii H 2000 *Phys. Rev.* B **61** 9475
[7] Woods J P, Patterson B M, Fernado A S, Jaswal S S, Welipitiya D and Sellmyer D J 1995 *Phys. Rev.* B **51** 1064
[8] Grandjean F and Long G J 1995 *Interstitial Intermetallic Alloys* (*NATO ASI Series E* vol 281) ed F Grandjean, G J Long and K H J Buschow (Dordrecht: Kluwer) chapter 19, p 463
[9] Long G J, Pringle O A, Grandjean F, Yelon W B and Buschow K H J 1993 *J. Appl. Phys.* **74** 504
Long G J, Pringle O A, Grandjean F and Buschow K H J 1992 *J. Appl. Phys.* **72** 4845
[10] Coehoorn R 1989 *Phys. Rev.* B **39** 13072
Coehoorn R 1990 *Phys. Rev.* B **41** 11790
Coehoorn R, Denissen C J M and Eppenga R 1991 *J. Appl. Phys.* **69** 6222
[11] Kalogirou O, Psycharis V, Saettas L and Niarchos D 1995 *J. Magn. Magn. Mater.* **146** 335
[12] Frank F C and Kasper J S 1958 *Acta Crystallogr.* **11** 184
Frank F C and Kasper J S 1959 *Acta Crystallogr.* **12** 483
[13] Watson R E and Weinert M 2001 *Solid State Physics* vol 56, ed H Ehrenreich and F Spaepen (London: Academic) pp 34–49

[14] Watson R E, Bennet L H and Melamud M 1988 *J. Appl. Phys.* **63** 3136
[15] Nelson D R 1983 *Phys. Rev.* B **28** 5515
[16] Kalogirou O, Psycharis V, Gjoka M and Niarchos D 1995 *J. Magn. Magn. Mater.* **147** L7
[17] Yelon W B and Hu Z 1996 *J. Appl. Phys.* **79** 1330
[18] Cadogan J M, Li H-S, Margarian A, Dunlop J B, Ryan D H, Collocott S J and Davis R L 1994 *J. Appl. Phys.* **76** 6138
[19] Hu Z and Yelon W B 1994 *Solid State Commun.* **91** 223
[20] Cao L Z, Shen J and Chen N X 2002 *J. Alloys Compounds* **336** 18
[21] Marsh R E 1995 *Acta Crystallogr.* B **51** 897
[22] Ibberson R M, Moze O, Jacobs T H and Buschow K H J 1991 *J. Phys.: Condens. Matter* **3** 1219
[23] Rodriquez-Carvajial J, Fernadez-Diaz M T and Martinez J L 1991 *J. Phys.: Condens. Matter* **3** 3215
[24] Hu Z, Yelon W B, Kalogirou O and Psycharis V 1996 *J. Appl. Phys.* **80** 2955
[25] Oleinek Ph, Isnard K, Convert P, Muller K-H, Loewenhaupt M and Schultz L 2000 *J. Alloys Compounds* **298** 220
[26] Courtois D, Li H-S and Cadogan J M 1996 *Solid State Commun.* **98** 565
[27] Téllez-Blanco J C, Kou X C and Grössinger R 1996 *J. Magn. Magn. Mater.* **164** L1
[28] Koch E and Fischer W 1996 *Z. Kristallogr.* **211** 251
[29] Bennet L H and Watson R E 1993 *J. Alloys Compounds* **197** 271
[30] Grandjean F, Ezekwenna P C, Long G J, Pringle O A, I'Heritier Ph, Ellouse M, Luo H P and Yelon W B 1998 *J. Appl. Phys.* **84** 1893
[31] Isnard O, Miraglia S, Soubeyroux J L and Fruchart D 1992 *Solid State Commun.* **81** 13
[32] Miraglia S, Soubeyroux J L, Kolbeck C, Isnard O, Fruchart D and Guillot M 1991 *J. Less-Common Met.* **171** 511
[33] Psycharis V, Kalogirou O, Devlin E, Gjoka M, Simopoulos A and Niarchos D 1996 *J. Magn. Magn. Mater.* **153** 75
[34] Melamud M, Bennet L H and Watson R E 1987 *J. Appl. Phys.* **61** 4246
[35] Melamud M, Bennet L H and Watson R E 1994 *J. Appl. Phys.* **76** 6044
[36] Li Z W, Zhou X Z and Morrish A H 1992 *J. Phys.: Condens. Matter* **4** 10409
[37] Moriya T 1979 *J. Magn. Magn. Mater.* **14** 1
Moriya T 1983 *J. Magn. Magn. Mater.* **31–34** 10
[38] Isnard O and Fruchart D 1994 *J. Alloys Compounds* **205** 1
[39] Yang F M, Han X-F, de Boer F R and Li H-S 1997 *J. Phys.: Condens. Matter* **9** 1339
[40] Ching W Y, Huang M-Z, Hu Z and Yelon W B 1997 *J. Appl. Phys.* **81** 5618
[41] Izumi H, Machida K and Adachi G 1997 *J. Alloys Compounds* **259** 191
[42] Ryan D H, Cadogan J M, Margarian A and Dunlop J B 1994 *J. Appl. Phys.* **76** 6150
[43] Kalogirou O, Psycharis V and Niarchos D 1996 *Solid State Commun.* **97** 471
[44] Hu B-P, Li H-S and Coey J M D 1990 *J. Appl. Phys.* **67** 4838
[45] Paoluzi A and Pareti L 1999 *J. Phys.: Condens. Matter* **11** 5613
[46] Yang D, Wang J, Tang N, Shen Y and Yanga F 1999 *Appl. Phys. Lett.* **74** 4020
[47] Huo G Y, Rao G H, Qiao Z Y, Liu Q L, Chen X L, Liang J K and Shen B G 2000 *J. Phys.: Condens. Matter* **12** 1161